DMD Fast Forward. Published on October 20, 2010 as doi:10.1124/dmd.110.036392

GENERATION OF HUMAN CHIRAL METABOLITES OF SIMVASTATIN AND LOVASTATIN BY BACTERIAL CYP102A1 MUTANTS

KEON-HEE KIM[1], JI-YEON KANG[1], DONG-HYUN KIM[1], SUN-HA PARK, SEON HA PARK, DOOIL KIM, KI DEOK PARK, YOUNG JU LEE, HEUNG-CHAE JUNG, JAE-GU PAN, TAEHO AHN, CHUL-HO YUN[2]

School of Biological Sciences and Technology, Chonnam National University, Gwangju 500-757, Republic of Korea (K.-H.K., J.-Y.K., D.-H.K., Su.-H.P., Se.H.P., C.-H.Y.); Gwangju Center, Korea Basic Science Institute, Gwangju 500-757, Republic of Korea (K.D.P., Y.J.L.); Systems Microbiology Research Center, Korea Research Institute of Bioscience and Biotechnology, Daejeon, Republic of Korea (D.K., H.-C.J., J.-G.P.); Department of Biochemistry, College of Veterinary Medicine, Chonnam National University, Gwangju, Republic of Korea (T.A.)

DMD Fast Forward. Published on October 20, 2010 as DOI: 10.1124/dmd.110.036392
This article has not been copyedited and formatted. The final version may differ from this version.

Running title: Oxidation of simvastatin and lovastatin by CYP102A1 mutants

Correspondence: Prof. Chul-Ho Yun, School of Biological Sciences and Technology, Chonnam National University, Gwangju 500-757, Republic of Korea; Tel: 82-62-530-2194; Fax: 82-62-530-2199; E-mail: chyun@jnu.ac.kr

Number of text pages: 30

Number of tables: 2

Number of figures: 7

Number of references: 40

Number of words in Abstract: 218

Number of words in Introduction: 697

Number of words in Discussion: 802

Abbreviations used: P450 or CYP, cytochrome P450; CYP102A1, cytochrome P450 BM3; CPR, NADPH-P450 reductase; CYP102A1, Cytochrome P450 BM3; IPTG, isopropyl-β-D-thiogalactopyranoside; TTN, total turnover number; MIST, metabolites in safety testing; HMG-CoA, 3-hydroxy-3-methylglutaryl-coenzyme A; FDA, Food and Drug Administration; K_s, spectrally determined dissociation constants; DLPC, L-α-dilauroyl-*sn*-glycero-3-phosphocholine; SIM, simvastatin; LOV, lovastatin; αNF, 7,8-benzoflavone; MD, molecular dynamics

DMD Fast Forward. Published on October 20, 2010 as DOI: 10.1124/dmd.110.036392
This article has not been copyedited and formatted. The final version may differ from this version.

Abstract

Recently, the wild-type and mutant forms of cytochrome P450 BM3 (CYP102A1) from *Bacillus megaterium* were found to oxidize various xenobiotic substrates, including pharmaceuticals, of human P450 enzymes. Simvastatin and lovastatin, which are used to treat hyperlipidemia and hypercholesterolemia, are oxidized by human P450 3A4/5 to produce several metabolites, including 6'β-OH, 3''-OH and exomethylene products. In this report, we show that the oxidation of simvastatin and lovastatin was catalyzed by wild-type CYP102A1 and a set of its mutants, which were generated by site-directed and random mutagenesis. One major hydroxylated product (6'β-OH) and one minor product (6'-exomethylene), but not other products, were produced by CYP102A1 mutants. Formation of the metabolites was confirmed by HPLC, LC-MS, and NMR. Chemical methods to synthesize the metabolites of simvastatin and lovastatin have not been reported. These results demonstrate that CYP102A1 mutants can be used to produce human metabolites, especially chiral metabolites, of simvastatin and lovastatin. Our computational findings suggest that a conformational change in the cavity of the mutant active sites is related to the activity change. The modeling results also suggest that the activity change results from the movement of several specific residues in the mutants' active sites. Furthermore, our computational findings suggest a correlation between the stabilization of the binding site and the catalytic efficiency of CYP102A1 mutants toward simvastatin and lovastatin.

Introduction

Simvastatin and lovastatin are well-known hyperlipidemia and hypercholesterolemia drugs that act as cholesterol-lowering agents (Caron et al., 2007). Simvastatin (marketed under the trade names ZOCOR, SIMLUP, SIMCARD, and SIMVACOR) is metabolized to at least four primary metabolites, namely 6'β-OH simvastatin, 6'-exomethylene simvastatin, 6'β-hydroxymethyl metabolite, and 3''-OH simvastatin (Fig. 1). Although CYP3A4 is the main enzyme involved in the primary metabolism of simvastatin, CYPs 2C8 (Tornio et al., 2005), 2C9 (Transon et al., 1996), and 2D6 (Transon et al., 1996) are also involved in the formation of simvastatin metabolites. The extensive oxidative metabolism of lovastatin (marketed under the trade names MEVACOR and ALTOPREV) in the human liver is primarily mediated by CYP3A enzymes, particularly CYP3A4, to generate three known metabolites, 6'β-OH lovastatin, 3''-OH lovastatin, and 6'-exomethylene (Garcia et al., 2003; Caron et al., 2007) (Fig. 2).

After oral ingestion, simvastatin and lovastatin, which are inactive lactones, are hydrolyzed to the corresponding β-hydroxyacid form (Vickers et al., 1990a). This molecule is a principal metabolite and an inhibitor of 3-hydroxy-3-methylglutaryl-coenzyme A (HMG-CoA) reductase. This enzyme catalyzes the conversion of HMG-CoA to mevalonate, which is an early and rate-limiting step in the biosynthesis of cholesterol. In addition to the P450-mediated oxidation and β-oxidation processes, glucuronidation constitutes a common metabolic pathway for statins (Prueksaritanont et al., 2002). The metabolites resulting from microsomal oxidation of

simvastatin (Vickers et al., 1990b) and lovastatin (Vyas et al., 1990) by P450 enzymes are effective inhibitors of HMG-CoA reductase. Therefore, it has been suggested that the metabolites may contribute to the cholesterol-lowering effect of simvastatin and lovastatin. However, systematic studies of the safety, efficacy, and toxicity of these metabolites have not been performed.

Recently, the Food and Drug Administration (FDA) modified its standards for evaluating drug toxicity, particularly with regard to the toxicity of drug metabolites. In February 2008, the FDA issued the Guidance for Industry: Safety Testing of Drug Metabolites: (http://www.fda.gov/downloads/Drugs/GuidanceComplianceRegulatoryInformation/Guidances/ucm079266.pdf).

According to these guidelines, any human drug metabolites "formed at greater than 10 percent of parent drug systemic exposure at steady state" should be subject to separate safety testing, which involves the synthesis and administration of these metabolites to test animals (Guengerich, 2009, and references therein). The issue of human metabolites in safety testing (MIST) has presented a challenge at the early stages of drug development for the pharmaceutical industry. Some metabolites of concern can be prepared by chemical methods, but others may not be easily prepared by these methods. In the latter cases, human liver microsomes, heterologously expressed human P450 enzymes in bacteria (Vail et al., 2005; Yun et al., 2006) and in insect cells (Rushmore et al., 2000), and purified human P450 enzymes are potential candidates for

biocatalysts to prepare human drug metabolites. However, these biocatalysts have several weaknesses, such as low catalytic activity and poor stability for industrial use (Guegerich 2002; Julsing et al., 2008).

The heme domain of P450 BM3 (CYP102A1) from *Bacillus megaterium*, which possesses monooxygenase activity, has strong similarities to eukaryotic members of the CYP4A (fatty acid hydroxylase) family. The P450 BM3 reductase domain, a mammalian-like diflavin reductase, is fused to the C terminus of the P450 domain in a single polypeptide. The fusion of these two enzymatic activities makes soluble CYP102A1 an ideal model for mammalian, particularly human, P450 enzymes. Recently, CYP102A1 mutants engineered through rational design or directed evolution were reported to produce human drug metabolites (Kim et al., 2008b, 2009, 2010; Park et al., 2010; Sawayama et al., 2009). In addition, CYP102A1 is a versatile monooxygenase with a demonstrated ability to catalyze a diversity of substrates and an established relevance to biotechnology (Julsing et al., 2008; Urlacher and Eiben, 2006; Yun et al., 2007, and references therein).

In this study, we evaluated whether CYP102A1 mutants could be used to produce the human metabolites of simvastatin and lovastatin. To our knowledge, the human metabolites of these statins have not been obtained by chemical synthesis and are not commercially available. Some of the tested mutations enabled the CYP102A1 enzyme to catalyze the oxidation of simvastatin and lovastatin to generate their human metabolites. Furthermore, computational

calculations and molecular modeling have been performed to provide further insight into molecular recognition on the basis of free energy decomposition and hydrogen-bond analysis.

Materials and Methods

Chemicals. Simvastatin and lovastatin were obtained from Merck (Rahway, NJ). NADPH was purchased from Sigma-Aldrich (St. Louis, MO, USA). Other chemicals were of the highest grade commercially available.

Construction of P450 BM3 mutants by site-directed mutagenesis. The CYP102A1 mutants used in this study were selected based on earlier work showing their increased catalytic activity toward several human substrates (Kim et al., 2008b, and references therein; Park et al., 2010). Each mutant bears amino acid substitution(s) relative to wild-type CYP102A1, as summarized in Supplemental Table S1.

Expression and purification of CYP102A1 mutants. Wild-type and mutant forms of CYP102A1 were expressed in *Escherichia coli* strain DH5αF'-IQ and purified as described previously (Kim et al., 2008b). The CYP102A1 concentrations were determined from CO-difference spectra using ε = 91 mM/cm. For all of the wild-type and mutated enzymes, a typical culture yielded 300 to 700 nM P450. The expression levels of wild-type and mutant CYP102A1 forms were typically in the range of 1.0 - 2.0 nmol P450/mg cytosolic protein.

Oxidation of simvastatin and lovastatin. Typical steady-state reactions for the oxidation of simvastatin and lovastatin included 50 pmol of CYP102A1 in 0.25 ml of 100 mM potassium phosphate buffer (pH 7.4) along with a specified amount of substrate. To determine the kinetic

parameters of several CYP102A1 mutants, 2 - 200 μM of statins was used. An aliquot of a NADPH-generating system was used to initiate reactions; final concentrations were 10 mM glucose 6-phosphate, 0.5 mM $NADP^+$, and 1 IU/ml yeast glucose 6-phosphate. A stock solution of statins (20 mM) was prepared in DMSO and diluted into the enzyme reactions with a final organic solvent concentration of < 1% (v/v). For the human CYP3A4 activity assay, a control experiment of 50 pmol P450, 100 pmol NADPH-P450 reductase (CPR), 100 pmol cytochrome b_5, and 45 μM L-α-dilauroyl-*sn*-glycero-3-phosphocholine (DLPC) in 0.25 ml of 100 mM potassium phosphate buffer (pH 7.4) was used instead of 50 pmol CYP102A1.

Reactions were generally incubated for 10 min at 37°C and terminated with a 2-fold excess of ice-cold dichloromethane. After centrifugation of the reaction mixture, the supernatant was carefully removed, and the solvent was evaporated under N_2 gas as described previously (Vickers et al., 1990b). The products were analyzed by HPLC using a Gemini C_{18} column (4.6 mm x 150 mm, 5 μm, Phenomenex, Torrance, CA) with an acetonitrile/water (70/30, v/v) mobile phase containing 2.5 mM formic acid. Eluates were detected by UV at 238 nm. Authentic metabolites of 6'β-OH and 6'-exomethylene were obtained by HPLC from reaction mixtures of simvastatin and lovastatin with human CYP3A4 as described below.

To determine the total turnover numbers (TTNs) of several P450 enzymes, a total of 1.0 mM of statin was used. The reaction in the presence of 500 μM of substrate and 50 pmol of enzyme was initiated by the addition of the NADPH-generating system in 0.25 ml of 100 mM

potassium phosphate buffer (pH 7.4) and incubated for 4 h at 37°C. After 2 h incubation, 500 μM of each substrate was added to the reaction mixture. The formation rate of statin metabolites was determined by HPLC as described above.

The kinetic parameters (K_m and k_{cat}) were determined using nonlinear regression analysis with GraphPad PRISM software (GraphPad, San Diego, CA). The data were fit to the standard Michaelis-Menten equation: $v = k_{cat}[E][S]/([S] + K_m)$, where the velocity of the reaction is a function of the turnover rate (k_{cat}), which is the rate-limiting step, the enzyme concentration ([E]), substrate concentration ([S]), and the Michaelis constant (K_m).

LC-MS analysis. CYP102A1 mutants and human CYP3A4 were incubated with 100 μM of lovastatin and simvastatin at 37°C for 30 min in the presence of an NADPH-generating system. Reactions were terminated by the addition of a 2-fold excess of ice-cold dichloromethane. After centrifugation, the supernatant from each incubated reaction was removed and evaporated to dryness. The reaction residue was reconstituted into 100 μl of mobile phase by vortex mixing and sonication for 20 sec. An aliquot (10 μl) of this solution was injected onto the LC column. LC–MS analysis was carried out in electrospray ionization (positive) mode on a Shimadzu LCMS-2010 EV system (Shimadzu Corporation, Japan) having LCMS solution software. The separation was performed on a Shim-pack VP-ODS column (2.0 mm i.d. × 250 mm, Shimadzu Corporation, Japan) using an acetonitrile/water (70/30, v/v) mobile phase containing 2.5 mM formic acid at a flow rate of 0.16 ml/min. To identify the metabolites, mass

spectra were recorded by electrospray ionization in positive mode. The interface and detector voltages were 4.4 kV and 1.5 kV, respectively. The nebulization gas flow was set at 1.5 l/min. The interface, curve desolvation line (CDL), and heat block temperatures were 250, 230, and 200°C, respectively.

Identification of the metabolites by NMR Spectroscopy. An Agilent model 1100 HPLC system was used for the isolation of the 6'β-OH metabolites of simvastatin and lovastatin in the reaction mixtures. Semi-preparative columns were used for the isolation of 6'β-OH simvastatin (Waters SunFire Prep C18, 5 μm, 10 mm i.d. × 150 mm) and 6'β-OH lovastatin (Varian Pursuit C18, 5 μm, 10 mm i.d. × 250 mm) from the reaction mixtures. Each metabolite mixture, which was about 10 mg in CH_3OH, was injected onto the semi-preparative columns. The 6'β-OH simvastatin was eluted with a linear gradient (1.5%/min) of 30-90% CH_3CN after elution with 30% CH_3CN for 10 min. The metabolite fractions were collected at 18.2 min. The 6'β-OH lovastatin was eluted with a series of gradients: H_2O:CH_3CN (75/25, v/v) for 20 min; 25-45% CH_3CN for 40 min (0.5%/min); 45-90% CH_3CN for 40 min (4.5%/min); and 90% CH_3CN for 10 min. The metabolite fractions were collected at 63.7 min. The flow rate was 3 ml/min for both columns, and the eluates were monitored at 240 nm.

NMR experiments were performed on a Varian VNMRS 600 MHz NMR spectrometer equipped with a carbon-enhanced cryogenic probe. Chloroform-d1 was used as a solvent, and chemical shifts for proton and carbon were measured in parts per million (ppm) relative to TMS.

DMD Fast Forward. Published on October 20, 2010 as DOI: 10.1124/dmd.110.036392
This article has not been copyedited and formatted. The final version may differ from this version.

All of the one-dimensional and two-dimensional NMR experiments were performed with standard pulse sequences in VNMR (v. 2.3) library and processed with the same software. Spectral assignments were done with one-dimensional ^{1}H- and ^{13}C- NMR spectroscopy along with two-dimensional NMR spectroscopic techniques (DQ-COSY, HSQC, HMBC). The stereochemical configurations of the 6'β-OH position of both compounds were determined with 1-dimensional NOESY.

Effects of 7,8-benzoflavone (αNF) on the oxidation reactions of simvastatin and lovastatin catalyzed by CYP102A1 enzymes. Reaction mixtures consisted of 50 pmol P450, 100 mM potassium phosphate buffer (pH 7.4), a NADPH-generating system, substrate (100 μM of simvastatin or lovastatin), and 200 μM αNF in 0.25 ml of 100 mM potassium phosphate buffer (pH 7.4). Products were analyzed by HPLC as described above. In the case of the human CYP3A4 activity assay, a control experiment of 50 pmol P450, 100 pmol NADPH-P450 reductase (CPR), 100 pmol cytochrome b_5, and 45 μM DLPC was used instead of 50 pmol CYP102A1.

Spectral binding titrations. Spectral binding titrations were used to determine dissociation constants (K_s) for substrates as previously described (Kim et al., 2008a). Binding affinities of ligands to the CYP102A1 enzymes were determined (at 23°C) by titrating 1.5 μM enzyme with the ligand in a total volume of 1.0 ml of 100 mM potassium phosphate buffer (pH 7.4). Final CH_3CN concentrations were < 2% (v/v). Spectral dissociation constants (K_s) were estimated

using GraphPad Prism software (GraphPad Software, San Diego, CA). Unless the estimated K_s was within 5-fold of the P450 concentration, nonlinear regression analysis was applied using the hyperbolic equation $\Delta A = B_{max}[L]/(K_s + [L])$, where A is the absorbance difference, B_{max} is the maximum absorbance difference extrapolated to infinite ligand concentration, and [L] is the ligand concentration.

Molecular dynamics and docking simulation. Coordinates of the CYP102A1 structure (PDB code: 2UWH) (Huang et al., 2007) from *B. megaterium* were taken from the Protein Data Bank (PDB). Crystallographic water molecules were removed from all of the structures. The structure 2UWH contains the mutated residue Phe82, which was corrected to Ala82. The rectified CYP102A1 was then mutated to CYP102A1 mutant #16 (R47L/F81I/F87V/E143G/L188Q/E267V) and CYP102A1 mutant #17 (R47L/E64G/F81I/F87V/E143G/L188Q/E267V) using MODELLER (Sali and Blundell, 1993). The substrates lovastatin (LOV) and simvastatin (SIM) were prepared for molecular dynamics simulation with CYP102A1 mutants. The substrates were then applied with partial atomic charges derived by fitting ESP obtained by quantum electronic structure calculation. The substrates were geometry optimized with the 6-31 G*(p, d) basis set by the B3LYP method using the Gaussian 03 program (Gaussian Inc., Wallingford, CT, USA). The Antechamber module was used to calculate the atom-centered restrained electrostatic surface potential (RESP) by fitting ESP estimated from wavefunctions (Bayly et al., 1993). Parameters that were missing for the

ligands were generated using the general amber force field (GAFF) and the Parmchk module of Antechamber (Wang et al., 2004). Docking was performed using AutoDock (Morris et al., 1998) to determine the correct position for the substates in place of palmitate. The best position was selected on the basis of the root-mean-square deviation (RMSD) and binding free energy. After applying the force field, all hydrogen atoms were automatically added to all systems. Structures were solvated with a TIP3P water model by creating an isometric water box, in which the distance of the box is 8.5 Å from the periphery of the protein (Jorgensen et al., 1983). Molecular systems were neutralized by the addition of counterions. Systems were then energy minimized in two steps. In the first step, the CYP102A1 and substrates were kept fixed, and only the water molecules were allowed to move; in the second step, all atoms were allowed to move. For the first step, the energy minimization was performed in 500 and 1500 steps using the steepest descent and conjugate gradient methods, respectively. For the second step, the energy minimizations were performed in 1000 and 1500 steps using the steepest descent and conjugate gradient methods, respectively. Heating was performed with a NVT ensemble for 10 ps; the CYP102A1 mutants complexed with substrates were restrained with a force constant of 10 kcal/mol/$Å^2$. Equilibration was performed for 50 ps on a NPT ensemble restraining the CYP102A1 mutants/substrates complex by 1 kcal/mol/$Å^2$. Final simulations, i.e., the production phase, were performed for 5 ns on a NPT ensemble at a temperature of 310 K and 1 atm of pressure. Step size was 2 fs for the entire simulation. A Langevin thermostat and barostat was

used for temperature and pressure coupling. A SHAKE algorithm was applied to constrain all bonds containing hydrogen atoms (van Gunsteren et al., 1977). The nonbonded cutoff was kept at 10 Å, and long-range electrostatic interactions were treated by the particle mesh Ewald (PME) method with a fast Fourier transform grid having approximately 0.1 nm space (Darden et al., 1993). Trajectory snapshots were taken at each 1 ps, which were then used for analysis. All simulations were performed by the SANDER module of AMBER 10 with amber force field (ff03) (Case et al., 2008).

Binding Free Energy Calculation. The Molecular Mechanics Poisson Boltzmann and Surface Area (MM/PBSA) methods were used to calculate binding free energies for all of the CYP102A1 mutant complexes, using MM/PBSA implementation in AMBER 10 (Massova and Kollman, 2000). Binding free energy (ΔG_{bind}) is given by the following equation: $\Delta G_{bind} = \Delta E_{MM} + \Delta G_{Sol} + T\Delta S$, where ΔG_{bind} is the binding free energy in solution, ΔE_{MM} is the molecular mechanics energy, which is comprised of a van der Waals and an electrostatic contribution, and ΔG_{Sol} is the solvation energy, which consists of electrostatic and nonpolar interactions. Entropy could be calculated by either normal-mode analysis or quasi-harmonic approximation. Estimation of entropy has been shown to be computationally expensive with a low prediction accuracy. In this study, $T\Delta S$ was not considered for the calculation, as we were mainly interested in protein flexibility and the relative energy contributions of amino acids toward binding. ΔE_{MM} was calculated by the following equation: $\Delta E_{MM} = \Delta E_{int\_elec} + \Delta E_{int\_vdW}$, where ΔE_{int_elec} and

ΔE_{int_vdW} are electrostatic and van der Waals interaction energies between substrates and CYP102A1 mutants. These energies were computed with no cutoff. The solvation energy ΔG_{Sol} can be divided into two parts: $\Delta G_{Sol} = \Delta G_{sol\_elec} + \Delta G_{sol\_npol}$. The electrostatic contribution to the solvation free energy ΔG_{sol_elec} was calculated using the generalized Born model (Gohlke and Case, 2004). The hydrophobic contribution to the solvation energy ΔG_{sol_npol} was determined with a function of the solvent accessible surface area by the following equation: $\Delta G_{sol\_npol} = \gamma SASA + b$, where γ and b are empirical constants. The γ value was set to 0.0072 kcal/mol/Å^2, while b was set to a default value of 0. SASA is the solvent accessible surface area estimated using the linear combination of pairwise overlaps (LCPO) model. Snapshots from 0.1 to 5 ns molecular dynamics (MD) simulation trajectories were taken for the calculation of free energy. For PBSA and GBSA calculations, dielectric constants for solute and solvent were taken as 1.0 and 80.0, respectively. SASA was calculated using the molsurf program implemented in AMBER 10 by taking the solvent probe as 1.4 Å. Free energy was decomposed using MM/PBSA of AMBER 10 to estimate the contribution of each residue in the binding process.

DMD Fast Forward. Published on October 20, 2010 as DOI: 10.1124/dmd.110.036392
This article has not been copyedited and formatted. The final version may differ from this version.

Results

Oxidation of simvastatin and lovastatin by wild-type P450 BM3 and its mutants. We examined whether CYP102A1 can oxidize simvastatin and lovastatin. First, the ability of wild-type and a set of CYP102A1 mutants to oxidize simvastatin and lovastatin was measured at a fixed substrate concentration (100 μM) (Fig. 3). While simvastatin and lovastatin are known to produce at least four and three metabolites, respectively (Fig. 1 and 2), CYP102A1 mutants produced only two metabolites, one major (6'β-OH statin) metabolite and one minor (6'-exomethylene statin) metabolite. The metabolites were analyzed by HPLC and compared to those of human CYP3A4 (Fig. 4 and 5). Catalytically active mutants of CYP102A1 produced one major product, which had a retention time that exactly matched the 6'β-OH statin, and the minor metabolite 6'-exomethylene product. However, other products were not observed under the experimental conditions used here.

The turnover numbers for the oxidation of statins (product formation) by the entire set of 18 mutants varied over a wide range. CYP102A1 wild-type showed very low catalytic activity towards simvastatin (0.0049 min^{-1} for 6'β-OH simvastatin) and no other metabolites were observed for either substrate. (Fig. 3). Mutant #4 did not show any apparent activity toward either statin (< 0.001 min^{-1}). Mutants #16 and #17 each showed higher activity than that of human CYP3A4. In the case of mutant #17, the turnover number (10 min^{-1}) was 3.3 and 2040-

fold higher than that of human CYP3A4 and wild-type CYP102A1, respectively.

Characterization of the chiral metabolites of simvastatin and lovastatin. The identities of the major metabolite and substrate were verified by comparing the HPLC results (Fig. 4 and 5), the LC/MS results (Supplemental Fig. S1 and S2), and the absorption spectra (Supplemental Fig. S3 and S4) with authentic compounds, which were produced by human CYP3A4. The production of 6'β-OH and 6'-exomethylene statins by CYP102A1 mutants was confirmed by LC-MS analysis of the reaction mixture. The retention time and fragmentation pattern of the CYP102A1 metabolites were exactly matched to those of the authentic metabolites, which were produced by human CYP3A4 (Supplemental Fig. S1 and S2).

Chemical structures of 6'β-OH statins were identified by one- and two-dimensional NMR experiments. Spectral assignments were accomplished with two-dimensional ^{1}H-NMR and ^{13}C-NMR spectroscopy along with two-dimensional NMR spectroscopic techniques. The results are shown in the Data Supplement (Supplemental Fig. S5; Supplemental Table S2 - S5). The stereochemical configurations of the 6'β-OH position for both compounds were determined with one-dimensional NOESY. There have been reports for proton chemical shifts in 6'β-OH lovastatin in different NMR solvents (acetonitrile-d4) (Vyas et al., 1990), and to our knowledge, there have been no publications of C13 chemical shift data for 6'β-OH simvastatin and 6'β-OH lovastatin. The stereochemical configurations at the 6'β-OH position of both compounds were determined with one-dimensional DPFGSE-NOE (Double Pulsed Field Gradient Spin Echo

NOE). When previously assigned proton peaks from H-6'α (δ 1.35 ppm for 6'β-OH simvastatin, δ 1.34 ppm for 6'β-OH lovastatin) were selectively irradiated, proton NMR peaks from H-7'(eq) (δ 2.44 ppm for 6'β-OH simvastatin, δ 2.43 ppm for 6'β-OH lovastatin) appeared out of two H-7' protons. Subsequent selective irradiation of H-8' using a one-dimensional DPFGSE-NOE experiment confirmed the 6'β-OH position of both compounds (Supplemental Fig. S5 E and F).

Simvastatin and lovastatin proved to be good substrates for CYP102A1 enzymes, exhibiting high turnover numbers that approached 10 and 18 min^{-1} for 6'β-OH product formation from simvastatin and lovastatin, respectively, in the case of mutant #17. Although other products were found to be metabolites of human liver microsomes (Caron et al., 2007, and references therein), all of the CYP102A1 enzymes, including wild-type and active mutants, produced only two metabolites, 6'β-OH and 6'-exomethylene (Fig. 4 and 5). Human CYP3A4, the major enzyme for the hydroxylation reactions of simvastatin and lovastatin in human liver, also shows a preference for the 6'β-hydroxylation reaction over the dehydrogenation reaction at the 6' position (Fig. 4 and 5).

Kinetic parameters of simvastatin and lovastatin oxidation by CYP102A1 mutants. The two high-activity mutants #16 and #17 were used to measure kinetic parameters for the 6'β-hydroxylation of simvastatin and lovastatin (Table 1; supplemental Fig. S6). Wild-type and some mutant forms of CYP102A1 did not exhibit any or appreciable activities to determine reliable

kinetic parameters (Fig. 3). Only mutants #16 and #17 showed significantly elevated k_{cat} values for the 6'β-hydroxylation reaction, which yielded the highest k_{cat} values of > 10 min^{-1} for simvastatin and lovastatin (Fig. 3). Human CYP3A4 exhibited k_{cat} values of 6.6 and 4.2 min^{-1} for 6'β-hydroxylation of simvastatin and lovastatin, respectively. The overall range of K_m values for the CYP102A1 mutants was from 37 to 44 μM. Notably, human CYP3A4 displayed a higher K_m value of 130 μM for the 6'β-hydroxylation of simvastatin. The catalytic efficiencies (k_{cat}/K_m) of 6'β-hydroxylation of simvastatin and lovastatin by mutant #17 were 0.36 and 0.46 $min^{-1}\cdot\mu M^{-1}$, which are more efficient than those of human CYP3A4 by 7- and 6-fold, respectively.

When the total turnover numbers (TTNs; mol product/mol catalyst) for the CYP102A1 mutants were determined, the overall range was 150 to 210 (Fig. 6). Mutant #16 showed the highest activity, which was 5~6-fold higher than that of human CYP3A4 following a 4-h incubation period. The wild-type CYP102A1 enzyme showed much lower catalytic activity towards simvastatin and lovastatin (0.77 and 1.9 nmol product/nmol P450, respectively).

Inhibitory effects of 7, 8-benzoflavone (αNF) on the CYP102A1 catalyzed oxidation of simvastatin and lovastatin. Modulation of the catalytic activities of human CYP3A4 by αNF is known (Ueng et al., 1997). In this work, we examined the effect of αNF on the catalytic activities of CYP102A1 mutants that possessed human CYP3A4 activities. αNF inhibited the 6'β-hydroxylation of simvastatin and lovastatin in a concentration-dependent manner. When 50 μM

of αNF was added to incubated reaction mixtures with simvastatin and lovastatin (Supplemental Fig. S7), the 6'β-hydroxylation activities of human CYP3A4 for simvastatin and lovastatin were inhibited by 42% and 69%, respectively. The 6'β-hydroxylation activities of CYP102A1 mutants #16 and #17 for simvastatin were inhibited by 44% and 77%, respectively. The activities of CYP102A1 mutants #16 and #17 for lovastatin were inhibited by 48% and 76%, respectively, in the presence of αNF. This result shows that αNF can bind to the active site of CYP102A1 mutants to change their catalytic activities.

A triple CYP102A1 mutant #10 (R47L/F87V/L188Q) has been reported to metabolize typical mammalian P450 substrates, such as amodiaquine, dextromethorphan, acetaminophen, testosterone, and 3,4-methylenedioxymethylamphetamine (van Vugt-Lussenburg et al., 2007). Although product formation from these chemicals by CYP102A1 mutant #10 was inhibited from 30 to 60% in the presence of αNF, αNF did not have a significant effect on the metabolism of acetaminophen and 3,4-methylenedioxymethylamphetamine (van Vugt-Lussenburg et al., 2007). This mutant could also oxidize simvastatin and lovastatin to generate 6'β-OH and 6'-exomethylene products at relatively low rates (Fig. 3: 6'β-OH simvastatin, 0.046 ± 0.003 min^{-1}; 6'-exomethylene simvastatin, 0.00028 ± 0.00068 min^{-1}; 6'β-OH lovastatin, 0.22 ± 0.17 min^{-1}; 6'-exomethylene lovastatin, 0.057 ± 0.008 min^{-1}).

Titration. The addition of simvastatin and lovastatin to a solution with human CYP3A4 produced a typical low- to high-spin conversion (Type I difference spectrum) (Supplemental Fig.

S8). The binding affinities of human CYP3A4 toward the simvastatin (K_s = 14 ± 1 μM) and lovastatin (K_s = 8.8 ± 0.8 μM) substrates were determined from the titration curves. However, in the case of the CYP102A1 mutants, the addition of the substrates tested here did not result in any apparent spectral changes (data not known).

Modeling and computational calculation. In this study, we have analyzed interactions in a dynamic environment that depend on time to derive more insight into molecular recognition. Interactions were analyzed on the basis of free energy decomposition and hydrogen-bond analysis. For each complex, free energy was decomposed to analyze the contributions of individual residues in binding. The hydrogen bonds that showed stable behavior during molecular dynamics were analyzed. To fully investigate the influence of the CYP102A1 mutation on the interaction with substrates, the substrate-residue interactions in each wild-type complex and the corresponding mutated complex were also compared systematically.

Docking and molecular dynamics simulation analysis. Binding features observed in the simulation of the substrates docked into the wide-type CYP102A1 (CYP102A1 WT) are schematically represented (Fig. 7 A and B) together with interatomic distances for the 6'β-carbon of the substrates and the Fe atom of the heme. Coordination of the substrates' 6'β -carbon to the catalytic iron atom was maintained for the entire simulation time, and none of the oxygen atoms in the substrates formed a stable hydrogen bond to any residues of CYP102A1 WT, suggesting that the substrate oxygen atoms are not the primary determinant; this situation for binding of

LOV (lovastatin)/SIM (simvastatin) into CYP102A1 WT is unlike the case of other CYP102A1 mutant complexes. Because no direct hydrogen bond between CYP102A1 WT and LOV/SIM was retained during the energy minimization stage of the initial complex model, the distance of the substrates' 6'β-carbon moved away from the catalytic iron atom during the equilibrium stage of the MD simulation (8-9 Å). In the subsequent data sampling stage, a direct hydrogen bond was also not observed. Significantly, the movement of the substrates from their original position at the catalytic sites to the channel entrance was observed in the MD simulation; this movement was found to be due to a collision between the fused ring connected to the oxooxane ring of LOV/SIM and flexible or large hydrophobic residues, such as Leu75 and Phe87. The simulations indicated that that the butanonate chain and oxooxane ring could not fit into the space created by the Thr49, Met185, and Leu437 shift without inducing steric repulsion. Thus, a small increase of the hydroxylation potency for SIM caused by introducing a methyl group on the LOV was only ascribed to the induced fit of SIM. Both simulations yield nearly identical mean values for the distance between the 6'β-carbon of the substrates and the Fe iron: 9.07 Å and 8.62 Å for LOV and SIM (Fig. 7 A and B), respectively, which are comparable to those observed in the experimental results described above.

The replacement of several residues [mutant #16 (R47L/F81I/F87V/E143G/L188Q/E267V) and mutant #17 (R47L/E64G/F81I/F87V/E143G/L188Q/E267V)] that led to quite potent monooxygenase activity induced significant changes of the overall shape of the catalytic sites of

CYP102A1, which were determined by the conformations of their side chains (Supplemental Fig. S9). The docking of substrates into CYP102A1 mutants (#16 and #17) revealed that coordination of the 6'β-carbon of the substrates to the iron atom is possible only when a hydrogen bond is made in the shallow cleft that acts as a catalytic subsite around the heme. The simulations for CYP102A1 WT and its mutant complexes showed a significant difference in the buried surface areas at the interface between the substrates and CYP102A1, suggesting that interaction of the hydrophobic residues in the catalytic subsites with the substrates is very extensive and consequently makes an important contribution to the destabilization of substrate binding. We speculate that the mutation of CYP102A1 causes conformational changes in the active site. When coupled with structural information, these conformational changes can be used to interpret the experimental results.

Hydrogen bonds play an essential role in stabilizing the complexes of the CYP102A1 mutants (#16 and #17): LOV/SIM complexes. We examined the geometry and stability of the hydrogen-bond network formed by LOV/SIM in the binding pocket of mutants #16/#17 on the basis of the trajectories of the MD simulations. Conformational changes in the binding pocket at the active site caused by several mutations affects the LOV and SIM binding (Fig. 7 C-F). Molecular surface visualization showed that there are relatively deep pockets in the CYP102A1 mutants. Interactions of these pockets with the oxooxane moiety of LOV/SIM could enhance their binding ability. The most significant hydrogen-bond contacts between the CYP102A1

mutants and LOV/SIM were schematically identified and characterized in terms of distances between heavy atoms and their percentage occurrence.

The hydroxyl group of the oxooxane ring in LOV complexed with CYP102A1 mutant #16 mainly participates in a hydrogen bond with the Ser72 hydroxyl group (87.3% occupied of the bonds being maintained during the MD simulation) (Fig. 7C). This hydrogen bond possibly plays an important role in enhancing the affinity of the oval-like pocket of CYP102A1 mutant #16. However, the hydroxyl of Ser72 adopted a different conformation in the SIM complex with CYP102A1 mutant #16 and failed to form a hydrogen bond with the hydroxyl group of SIM; it is present in only 17.0% of the computed snapshots (Fig. 7D), indicating that SIM barely interacts with Ser72 in the CYP102A1 mutant #16 active site model. The hydrophobic interaction between the methyl butanoate group and Ile263/Ala264 was shown to contribute to the complex stabilization, while the hydrogen bond to Ser72 was frequently observed to be cleaved in the simulation, giving a longer average distance than that for the complex with LOV.

In the model structure of CYP102A1 mutant #17 complex with LOV, Ala330 and Leu437 make a hydrogen bond and an electrostatic interaction through their backbone carbonyl group with a hydroxyl group and carbonyl group located in the oxooxane ring, respectively (95.3% occupied for Leu437 and 91.6% occupied for Ala330). These interactions may stabilize the binding of LOV to CYP102A1 mutant #17. The averaged distances along the 5 ns MD trajectory

between the 6'β carbon atom of LOV and the Fe atom of the heme is below 2.77 Å (Fig. 7E). For the SIM complex with CYP102A1 mutant #17, no interaction exists between the main chain oxygen of the Ala330 backbone and the carbonyl group of the oxooxane ring in SIM (Fig. 7F), but another hydrogen bond forms between the main chain oxygen of the Leu437 backbone and the hydroxyl group of the SIM oxooxane ring (86.0% occupied). This hydrogen bond may also result in the different conformation for bound SIM (Fig. 7F).

The hydrogen bond and the electrostatic interaction in the CYP102A1 mutant #17/LOV make significant contact with the substrate compared to complexes of mutant #16/LOV, mutant #17/SIM, and mutant #16/SIM. According to our newly described binding mode, the carbonyl group of the Ala330 backbone forms a strong electrostatic interaction with the carbonyl group of the oxooxane ring in LOV, whereas similar interaction does not exist in other complexes. The difference in the hydrogen bonding and electrostatic interaction reveals that LOV binds most strongly with CYP102A1 mutant #17, which explains the significantly higher catalytic activity of the CYP102A1 mutant #17/LOV complex compared to that of other complexes. The large changes at position Leu437 are expected to account for the reduction in favorable interaction of LOV/SIM with CYP102A1 mutant #16 and SIM with CYP102A1 mutant #17 compared to LOV with CYP102A1 mutant #17.

Interestingly, in CYP102A1 mutant #16 complexed with LOV and SIM, the main chain

oxygen atoms of Ala330 and Leu437 lose significant the hydrogen bond and the electrostatic interaction compared with the CYP102A1 mutant #17 complexes. There is a particularly large difference in orientations of the side chains of Ala330 and Leu437. Rotations occur at the side chains of Ala330/Leu437, which are correlated with changes in the distances of the 6'β-carbon in the substrates from the heme iron. This alteration in the side chain orientation of the active site residues also implies different interactions between the substrates and the CYP102A1 mutants. Simulations also showed that the butanoate moiety did not form any hydrogen bonds to the enzyme. Thus, the oxooxane ring can play an important role in binding the substrate not only by forming the hydrogen bond and the electrostatic interaction to the enzyme but also by properly directing the hydrophobic substituent to the catalytic subsite and enabling it to enter the cavity more fully.

Free energy calculation. To evaluate the different contributions to the binding free energy of LOV/SIM with CYP102A1 WT and the highly active mutants #16/#17, absolute binding free energies were calculated for four complexes using the MMPBSA method. The investigation into the forces involved in substrate binding can also be obtained by analyzing the MM/PBSA free energy contributions, which are listed in Table 2 for six complexes. In the present study, we estimated the different components of interaction energy that contribute to substrate binding. These include van der Waals, electrostatic, polar solvation, and nonpolar solvation interaction energies. The entropy was not calculated as we are only interested in the relative binding free

energy. The calculated ΔG_{bind} for the mutant #17/LOV complex (-19.49 kcal/mol) was the most negative among the ΔG_{bind} values for all complexes. This result agrees with the previous experimental results, which shows that the energetic analysis performed by MM-PB(GB)SA is applicable to the current case study.

The binding free energy of the mutant complexes #16/LOV, #17/LOV, #16/SIM, and #17/SIM increased by -12.75, -16.76, -9.01, and -10.56 kcal/mol with respect to the corresponding WT/substrate complex, which indicates that the two mutants #16/#17 bind more strongly to LOV/SIM than WT does. This also suggests that mutants #16 and #17 exhibit substrate acceptance for LOV/SIM. Comparisons of the free energy components between the WT complex and each mutant complex were carried out to elucidate the mechanism driving substrate acceptance. The differences of the non-polar solvation energies among the six complexes are relatively small, which indicates that better cavity packing is retained in the mutated complexes. There is a decrease of electrostatic and van der Waals energies in the WT complex of about 35-70 and 15-22 kcal/mol for the LOV and SIM complexes relative to the respective CYP102A1 mutants, which should be essential to the rejection of CYP102A1 WT for LOV/SIM.

Intermolecular van der Waals and electrostatic interactions are both important contributions to substrate binding. Nonpolar solvation terms, which correspond to the burial of solvent

DMD Fast Forward. Published on October 20, 2010 as DOI: 10.1124/dmd.110.036392
This article has not been copyedited and formatted. The final version may differ from this version.

accessible surface area upon binding of substrates to the active sites of mutants, contribute slightly favorably. The gas-phase electrostatic values, ΔE_{int_elec}, for the four complexes show that electrostatic interactions are in favor of the binding; however, the overall electrostatic interactions energies, ΔG_{Sol} ($\Delta E_{int\_elec}+\Delta G_{sol\_elec}$) are positive and unfavorable for the binding, which is caused by the large desolvation penalty for charged and polar groups that is not sufficiently compensated for upon complex formation. Comparing the van der Waals/nonpolar ($\Delta E_{int\_vdW}+\Delta G_{sol\_npol}$) contributions with the electrostatic contributions ΔG_{Elec}, we find that the association between LOV/SIM and mutants #16/#17 is mainly driven by more favorable van der Waals/nonpolar interactions in the complex than in solution. The electrostatic interactions between mutants #16/#17 and the butanonate chain are strong, but the electrostatic interactions between the solvent (water molecules) and the substrates are much stronger. Thus, when a substrate transfers from the solvent to the binding pocket, the electrostatic contributions for the butanonate moiety are unfavorable to substrate binding. The terminal butanyl chain of LOV/SIM is sandwiched between the side chains of Leu75 and Val78 and makes hydrophobic and van der Waals interactions with the side chains of Ala82 and Val87. Overall, this suggests that the affinities of the two substrates for the two mutants #16/#17 are dominated by shape complementarity, but the total affinity arises from a more complex interplay between all of these energy components. The structural analysis demonstrates that the hydrophobic group in the upper part of the heme takes advantage of the favorable van der Waals and hydrophobic interactions

with the binding pocket of CYP102A1 mutants. In the binding pocket, Leu75, Val78, Ala82, Val87, Ile263, and Leu437 residues constitute a relatively large hydrophobic core, which can generate strong van der Waals and hydrophobic interactions with the fused ring of the substrates. The ΔE_{int_vdW} value for the complex of mutants #17 with LOV is the highest among the complexes of mutants #16/#17 with the two substrates because lovastatin fits more snugly within the active site cavity and binds more tightly to mutant #17 than to the other complexes by adding nonpolar packing to the active site to a much greater extent.

Discussion

In this work, we have shown that bacterial CYP102A1 mutant enzymes catalyze the same reactions as human CYP3A4 to generate the human metabolites 6'β-OH and 6'-exomethylene from simvastatin and lovastatin. To our knowledge, the production of metabolites of simvastatin and lovastatin by chemical synthesis has never been reported. The 6'β-OH products are chiral compounds, which are usually difficult to synthesize by chemical methods. Therefore, an alternative to chemical synthesis of these metabolites is to use CYP102A1 enzymes to generate the metabolites of simvastatin and lovastatin. Interestingly, an unknown P450 from *Nocardia autotropica* has been found to oxidize simvastatin to generate 6'β-hydroxymethyl simvastatin (Gbewonyo et al., 1991).

Human P450 enzymes are involved in the metabolism of most (> 80%) drugs currently available on the market (Guengerich, 2003). Previously, we have proposed that CYP102A1 from *B. megaterium* could be developed as a biocatalyst with comparable drug oxidation activities to human P450 (Yun et al., 2007, and references therein). In recent studies, several lines of evidence supporting our proposal have been published. CYP102A1 mutants were found to generate human drug metabolites by oxidizing various drugs, including clozapine (Damsten et al., 2008), diclofenac (Damsten et al., 2008), acetaminophen (Damsten et al., 2008), 3,4-methylenedioxymethylamphetamine (Stjernschantz et al., 2008), dextromethorphan (Stjernschantz et al., 2008), phenacetin (Kim et al., 2010), verapamil (Sawayama et al., 2009),

and andastemizole (Sawayama et al., 2009). CYP102A1 mutants can also oxidize several human P450 substrates, including 7-ethoxycoumarin (Kim et al., 2008b), coumarin (Park et al., 2010), chlorzoxazone (Park et al., 2010), and resveratrol (Kim et al., 2009), to generate human metabolites.

The issue of human metabolites in safety testing (MIST) as outlined by the FDA has presented a challenge at the early stages of drug development for the pharmaceutical industry (Guengerich, 2009, and references therein). Metabolites of concern should be prepared by chemical methods or with biocatalysts, such as bacteria, yeast, and enzymes. Human drug metabolites are required for studies of drug toxicity, especially to satisfy the MIST issue, and efficacy during the process of drug discovery and development. The “active metabolite” is also an important issue in drug development (Johnson et al., 2004). In addition to the use of CYP102A1 mutants for the production of the metabolites of human P450-catalyzed reactions, we found other advantages to using CYP102A1 mutants instead of human P450 enzymes. For example, the human metabolite piceatannol can be generated from the anti-cancer preventive agent resveratrol by CYP102A1 (Kim et al., 2009); however, piceatannol cannot be made from its substrate, resveratrol, by human P450 enzymes, as piceatannol is a potent inhibitor for the human P450 catalyzed reactions.

Several CYP102A1 mutants were generated by directed evolution and rational design and were found to have much higher activity and stability than human P450 enzymes. These mutants could thus be developed as industrial enzymes for cost-effective and scalable production of human drug metabolites. The metabolites could also be developed as lead compounds for new drugs.

Our computational findings suggest that a conformational change in the cavity size of the mutant active sites is related to the activity change. The modeling results further suggest that the changes in activity result from the movement of several specific residues in the mutant active sites (Fig. 7; supplemental Fig. S9). The computational results obtained from highly active mutants with the statins are consistent with that of previous work for CYP102A1 mutants with phenacetin/7-ethoxyresorufin (Kim et al., 2010).

We also could find a good correlation between *in silico* analyses and *in vitro* determination of k_{cat} values of CYP102A1 mutants. Mutants #17 showed higher k_{cat} values than those of mutant #16 towards lovastatin and simvastatin (Table 1). Calculated binding free energies of mutant #17/SIM and mutant #17/LOV complexes were greater than those of mutant #16/SIM and mutant #16/LOV complexes, respectively (Table 2). When the average distances between the 6'β carbon atom of statins and the Fe atom were compared, mutant #17 showed much shorter average distances than those of mutant #16. However, we could not see apparent differences of K_m values between the complexes when experimental error ranges were considered (Table 1).

In summary, this work involved a set of CYP102A1 mutants and statin substrates, which are human P450 substrates, and revealed that bacterial CYP102A1 enzymes catalyze the same reactions as human CYP3A4 to generate the human metabolites 6'β-OH and 6'-exomethylene. The oxidation of simvastatin and lovastatin is catalyzed by wild-type and some mutant forms of CYP102A1. One major hydroxylated product, the 6'β-OH product, was produced as a result of a hydroxylation reaction. The other product, the exomethylene product, was produced by a dehydrogenation reaction. Metabolite formation was confirmed by HPLC and LC-MS by comparing the metabolites to the authentic human metabolites produced by human CYP3A4. Chemical structures of the major 6'β-OH products were identified by NMR. Thus, the CYP102A1 mutants efficiently produce human metabolites of simvastatin and lovastatin.

Authorship Contribution

Participated in research design: K.H. Kim, D. Kim, Jung, Pan, Ahn, and Yun

Conducted experiments: K.H. Kim, Kang, D.H. Kim, Su.H. Park, Se.H. Park, K.D. Park, and Lee

Performed data analysis: K.H. Kim, Kang, D.H. Kim, Su.H. Park, Se.H. Park, D. Kim, K.D. Park, Lee, Jung, Pan, Ahn, and Yun

Wrote or contributed to the writing of the manuscript: D. Kim, K.D. Park, and Yun

References

Bayly CI, Cieplak P, and Cornell WDK (1993) A well-behaved electrostatic potential based method using charge restraints for deriving atomic charges: the RESP Model. *J Phys Chem* **97:**10269-10280.

Caron G, Ermondi G, and Testa B (2007) Predicting the oxidative metabolism of statins: an application of the MetaSite algorithm. *Pharm Res* **24:**480-501.

Case DA, Darden TA, Cheatham III TE, Simmerling CL, Wang J, Duke RE, Luo R, Crowley M, Walker RC, Zhang W, Merz KM, Wang B, Hayik S, Roitberg A, Seabra G, Kolossváry I, Wong KF, Paesani F, Vanicek J, Wu X, Brozell SR, Steinbrecher T, Gohlke H, Yang L, Tan C, Mongan J, Hornak V, Cui G, Mathews DH, Seetin MG, Sagui C, Babin V, and Kollman PA (2008), AMBER 10, University of California, San Francisco.

Damsten MC, van Vugt-Lussenburg BM, Zeldenthuis T, de Vlieger JS, Commandeur JN, and Vermeulen NP (2008) Application of drug metabolising mutants of cytochrome P450 BM3 (CYP102A1) as biocatalysts for the generation of reactive metabolites. *Chem Biol Interact* **171**:96-107.

Darden T, York D, and Pedersen L (1993) Particle mesh ewald: An N.Log (N) method for computing ewald sums. *J Chem Phys* **98:**10089-10092.

García MJ, Reinoso RF, Sánchez Navarro A, and Prous JR (2003) Clinical pharmacokinetics of statins. *Methods Find Exp Clin Pharmacol* **25:**457-481.

Gbewonyo K, Buckland BC, and Lilly MD (1991) Development of a largescale continuous substrate feed process for the biotransformation of simvastatin by Nocardia sp. *Biotechnol Bioeng* **37:**1101-1107.

Gohlke H and Case DA (2004) Converging free energy estimates: MM-PB (GB) SA studies on the protein-protein complex Ras-Raf. *J Comput Chem* **25:**238–250.

Guengerich FP (2002) Cytochrome P450 enzymes in the generation of commercial products. *Nat Rev Drug Discov* **1:**359-366.

Guengerich FP (2003) Cytochromes P450, drugs, and diseases. *Mol Interv* **3:**194-204.

Guengerich FP (2009) Introduction: Human metabolites in safety testing (MIST) issue. *Chem Res Toxicol* **22:**237-238.

Huang WC, Westlake AC, Maréchal JD, Joyce MG, Moody PC, and Roberts GC (2007) Filling a hole in cytochrome P450 BM3 improves substrate binding and catalytic efficiency. *J Mol Biol* **373:**633-651.

Johnson MD, Zuo H, Lee KH, Trebley JP, Rae JM, Weatherman RV, Desta Z, Flockhart DA, and

Skaar TC (2004) Pharmacological characterization of 4-hydroxy-*N*-desmethyl tamoxifen, a novel active metabolite of tamoxifen. *Breast Cancer Res Treat* **85:**151-159.

Jorgensen WL, Chandrasekhar J, Madura JD, Impey RW, and Klein ML (1983) Comparison of simple potential Ffunctions for simulating liquid water. *J Chem Phys* **79:**926-935.

Julsing MK, Cornelissen S, Bühler B, and Schmid A (2008) Heme-iron oxygenases: powerful industrial biocatalysts? *Curr Opin Chem Biol* **12:**177-186.

Kim DH, Ahn T, Jung HC, Pan JG, and Yun CH (2009) Generation of the human metabolite piceatannol from the anti-cancer preventive agent resveratrol by bacterial cytochrome P450 BM3. *Drug Metab Dispos* **37:**932-936.

Kim DH, Kim KH, Isin EM, Guengerich FP, Chae HZ, Ahn T, and Yun CH (2008a) Heterologous expression and characterization of wild-type human cytochrome P450 1A2 without conventional N-terminal modification in *Escherichia coli*. *Protein Expr Purif*. **57:**188-200.

Kim DH, Kim KH, Kim D, Jung HC, Pan JG, Chi YT, Ahn T, and Yun CH (2010) Oxidation of human cytochrome P450 1A2 substrates by Bacillus megaterium cytochrome P450 BM3. *J Mol Catal B: Enzym* **63:**179-187.

Kim DH, Kim KH, Kim DH, Liu KH, Jung HC, Pan JG, and Yun CH (2008b) Generation of

human metabolites of 7-ethoxycoumarin by bacterial cytochrome P450 BM3. *Drug Metab Dispos* **36:**2166-2170.

Massova I and Kollman PA (2000) Combined molecular mechanical and continuum solvent approach (MM-PBSA/GBSA) to predict ligand binding. *Perspect Drug DiscoVery Des* **18:**113-135.

Morris GM, Goodsell DS, Halliday RS, Huey R, Hart WE, Belew RK, and Olson AJ (1998) Automated docking using a Lamarckian genetic algorithm and an empirical binding free energy function. *J Comput Chem* **19:**1639-1662.

Park SH, Kim DH, Kim D, Kim DH, Jung HC, Pan JG, Ahn T, Kim D, and Yun CH (2010) Engineering bacterial cytochrome P450 (P450) BM3 into a prototype with human P450 enzyme activity using indigo formation. *Drug Metab Dispos* **38:**732-739.

Prueksaritanont T, Subramanian R, Fang X, Ma B, Qiu Y, Lin JH, Pearson PG, and Baillie TA (2002) Glucuronidation of statins in animals and humans: a novel mechanism of statin lactonization. *Drug Metab Dispos* **30:**505-512.

Rushmore TH, Reider PJ, Slaughter D, Assang C, and Shou M (2000) Bioreactor systems in drug metabolism: Synthesis of cytochrome P450-generated metabolites. *Metab Eng* **2:**115-125.

Sali A and Blundell TL (1993) Comparative protein modelling by satisfaction of spatial

restraints. *J Mol Biol* **234:**779–815.

Sawayama AM, Chen MM, Kulanthaivel P, Kuo MS, Hemmerle H, Arnold FH (2009) A panel of cytochrome P450 BM3 variants to produce drug metabolites and diversify lead compounds. *Chemistry* **15:**11723-11729.

Stjernschantz E, van Vugt-Lussenburg BM, Bonifacio A, de Beer SB, van der Zwan G, Gooijer C, Commandeur JN, Vermeulen NP, and Oostenbrink C (2008) Structural rationalization of novel drug metabolizing mutants of cytochrome P450 BM3. *Proteins* **71**:336-352.

Transon C, Leemann T, Dayer P (1996) In vitro comparative inhibition profiles of major human drug metabolising cytochrome P450 isozymes (CYP2C9, CYP2D6 and CYP3A4) by HMG-CoA reductase inhibitors. *Eur J Clin Pharmacol* **50:**209-215.

Tornio A, Pasanen MK, Laitila J, Neuvonen PJ, Backman JT (2005) Comparison of 3-hydroxy-3-methylglutaryl coenzyme A (HMG-CoA) reductase inhibitors (statins) as inhibitors of cytochrome P450 2C8. *Basic Clin Pharmacol Toxicol* **97:**104-108.

Ueng YF, Kuwabara T, Chun YJ, and Guengerich FP (1997) Cooperativity in oxidations catalyzed by cytochrome P450 3A4. *Biochemistry* **36:**370-381.

Urlacher VB and Eiben S (2006) Cytochrome P450 monooxygenases: perspectives for synthetic application. *Trends Biotechnol* **24:**324-330.

van Gunsteren WF and Berendsen HJC (1977) Algorithms for macromolecular dynamics and constraint dynamics. *Mol Phys* **34:**1311–1327.

van Vugt-Lussenburg BM, Stjernschantz E, Lastdrager J, Oostenbrink C, Vermeulen NP, and Commandeur JN (2007) Identification of critical residues in novel drug metabolizing mutants of cytochrome P450 BM3 using random mutagenesis. *J Med Chem* **50:**455-461.

Vail RB, Homann MJ, Hanna I, and Zaks A (2005) Preparative synthesis of drug metabolites using human cytochrome P450s 3A4, 2C9 and 1A2 with NADPH-P450 reductase expressed in *Escherichia coli*. *J Ind Microbiol Biotechnol* **32:**67-74.

Vickers S, Duncan CA, Chen IW, Rosegay A, and Duggan DE (1990a) Metabolic disposition studies on simvastatin, a cholesterol-lowering prodrug. *Drug Metab Dispos* **18:**138-145.

Vickers S, Duncan CA, Vyas KP, Kari PH, Arison B, Prakash SR, Ramjit HG, Pitzenberger SM, Stokker G, and Duggan DE (1990b) In vitro and in vivo biotransformation of simvastatin, an inhibitor of HMG CoA reductase. *Drug Metab Dispos* **18:**476-483.

Vyas KP, Kari PH, Pitzenberger SM, Halpin RA, Ramjit HG, Arison B, Murphy JS, Hoffman WF, Schwartz MS, Ulm EH, and Duggan DE (1990) Biotransformation of lovastatin. I. Structure elucidation of in vitro and in vivo metabolites in the rat and mouse. *Drug Metab Dispos* **18:**203-211.

Wang J, Wolf RM, Caldwell JW, Kollman PA, and Case DA (2004) Development and testing of a general amber force field. *J Comput Chem* **25:**1157-1174.

Yun CH, Kim KH, Kim DH, Jung HC, and Pan JG (2007) The bacterial P450 BM3: a prototype for a biocatalyst with human P450 activities. *Trends Biotechnol* **25:**289-298.

Yun CH, Yim SK, Kim DH, and Ahn T (2006) Functional expression of human cytochrome P450 enzymes in *Escherichia coli*. *Curr Drug Metab* **7:**411-429.

FOOTNOTES

This work was supported in part by the 21C Frontier Microbial Genomics and the Application Center Program of the Ministry of Education, Science & Technology (MEST) of the Republic of Korea; by the National Research Foundation [Grant 2010-0027685]; by the Second Stage BK21 Project from the MEST of the Republic of Korea; and by the Support Program for the Advancement of National Research Facilities and Equipment of the MEST, Republic of Korea (2010).

Some parts of the work have been presented at the 16th North American Regional ISSX Meeting, Baltimore, Maryland, USA, October 18–22, 2009: Kang JY, Kim KH, Kim DH, Jung HC, Pan JG, Ahn T, Yun CH (2009) Generation of Human Metabolites of Simvastatin and Lovastatin by Bacterial Cytochrome P450 BM3 Enzymes [abstract]. *Drug Metab. Rev.* **41 (supplement 3):** 47.

[1]These authors are contributed equally to this work.

[2]*Correspondence*: Prof. Chul-Ho Yun, School of Biological Sciences and Technology, Chonnam National University, Gwangju 500-757, Republic of Korea; Tel: 82-62-530-2194; Fax: 82-62-530-2199; E-mail: chyun@jnu.ac.kr

Legends for Figures

Fig. 1. Structures of simvastatin and its human metabolites. The formation of metabolites is catalyzed by P450 enzymes in the presence of NADPH in the human liver.

Fig. 2. Structures of lovastatin and its human metabolites. The formation of metabolites is catalyzed by P450 enzymes in the presence of NADPH in the human liver.

Fig. 3. Rates of 6'β-OH product formation by various CYP102A1 mutants. Assays were performed using 100 μM simvastatin or lovastatin as described in the "Materials and Methods." Values are the mean ± SD of triplicate determinations.

Fig. 4. HPLC chromatograms of simvastatin metabolites produced by CYP102A1 mutants (#13 ~ #17) and human CYP3A4. Peaks were identified by comparing the retention times with those of metabolites produced by CYP3A4. The peaks of the substrate and two major products (hydroxylated product and exomethylene product) are indicated. UV absorbance was monitored at 238 nm.

Fig. 5. HPLC chromatograms of lovastatin metabolites produced by CYP102A1 mutants (#13 - #17) and human CYP3A4. Peaks were identified by comparing the retention times with those of substrate and authentic metabolites produced by CYP3A4. The peaks of the substrate and two major products are indicated. UV absorbance was monitored at 238 nm.

Fig. 6. Total turnover numbers for 6'β-OH product formation by CYP102A1 mutants. To determine the total turnover number of several CYP102A1 mutants, we used 1.0 mM of simvastatin or lovastatin. The reaction was initiated by the addition of the NADPH-generating system and incubation for 4 h at 37ºC. The formation rate of metabolites was determined by HPLC as described in Figures 4 and 5.

Fig. 7. Molecular binding surface area and binding site structural comparison of lovastatin and simvastatin in wild-type CYP102A1 (WT) and its mutants (#16 and #17); the average MD structures of (A) WT/lovastatin, (B) WT/simvastatin, (C) mutant #16/lovastatin, (D) mutant #16/simvastatin, (E) mutant #17/lovastatin, and (F) mutant #17/simvastatin are shown. The substrate, heme, and active sites are shown as stick diagrams.

DMD Fast Forward. Published on October 20, 2010 as DOI: 10.1124/dmd.110.036392
This article has not been copyedited and formatted. The final version may differ from this version.

TABLE 1.

Kinetic parameters for the formation of the 6'β-OH hydroxylated product by CYP102A1 mutants

P450 enzyme	Simvastatin			Lovastatin		
	k_{cat} (min^{-1})	K_m (μM)	k_{cat}/K_m ($min^{-1}/\mu M$)	k_{cat} (min^{-1})	K_m (μM)	k_{cat}/K_m ($min^{-1}/\mu M$)
Mutant #16	10 ± 1	37 ± 6	0.27 ± 0.05	14 ± 1	44 ± 9	0.32 ± 0.07
Mutant #17	15 ± 1	42 ± 6	0.36 ± 0.60	19 ± 2	41 ± 9	0.46 ± 0.11
Human CYP3A4	6.6 ± 0.9	130 ± 30	0.051 ± 0.014	4.2 ± 0.5	54 ± 15	0.078 ± 0.024

TABLE 2.

Individual energy components for the calculated binding free energies of lovastatin/simvastatin complexed with CYP102A1 wild-type (WT) and its two mutants, mutant #16 (M16) (R47L/F81I/F87V/E143G/L188Q/E267V) and mutant #17 (M17) (R47L/E64G/F81I/F87V/E143G/L188Q/E267V).

Energy	**WT/lovastatin**	**WT/simvastatin**	**M16/lovastatin**	**M16/simvastatin**	**M17/lovastatin**	**M17/simvastatin**
ΔE_{int_elec}	-6.79 ± 0.65	-7.20 ± 0.28	-38.48 ± 0.26	-80.12 ± 0.57	-48.03 ± 0.28	-73.92 ± 0.43
ΔE_{int_vdW}	-4.94 ± 0.18	-4.14 ± 0.18	-27.01 ± 0.19	-19.89 ± 0.19	-28.64 ± 0.17	-19.54 ± 0.21
ΔG_{sol_npol}	-0.55 ± 0.17	-0.62 ± 0.04	-3.16 ± 0.02	-4.57 ± 0.01	-4.16 ± 0.09	-3.66 ± 0.02
ΔG_{sol_elec}	9.55 ± 0.25	9.05 ± 0.19	54.17 ± 0.23	92.65 ± 0.43	60.33 ± 0.22	83.64 ± 0.38
ΔG_{Sol}	9.76 ± 0.16	8.42 ± 0.25	55.34 ± 0.24	88.07 ± 0.42	56.18 ± 0.27	79.99 ± 0.31
ΔG_{Elec}	2.76 ± 0.02	1.84 ± 0.06	15.68 ± 0.21	12.54 ± 0.22	12.31 ± 0.15	9.72 ± 0.27
ΔG_{bind}	-2.73 ± 0.23	-2.92 ± 0.04	-15.48 ± 0.24	-11.93 ± 0.24	-19.49 ± 0.18	-13.48 ± 0.23

ΔG_{Sol} is the polar/nonpolar ($\Delta G_{sol\_elec}+\Delta G_{sol\_npol}$) contribution. ΔG_{Elec} is the electrostatic ($\Delta E_{int\_elec}+\Delta G_{sol\_elec}$) contribution. All energies are averaged over 200 snapshots and are given in kcal/mol. Calculation of ΔG_{bind} does not explicitly consider entropy contributions. The values represent the mean ± S.E.M.

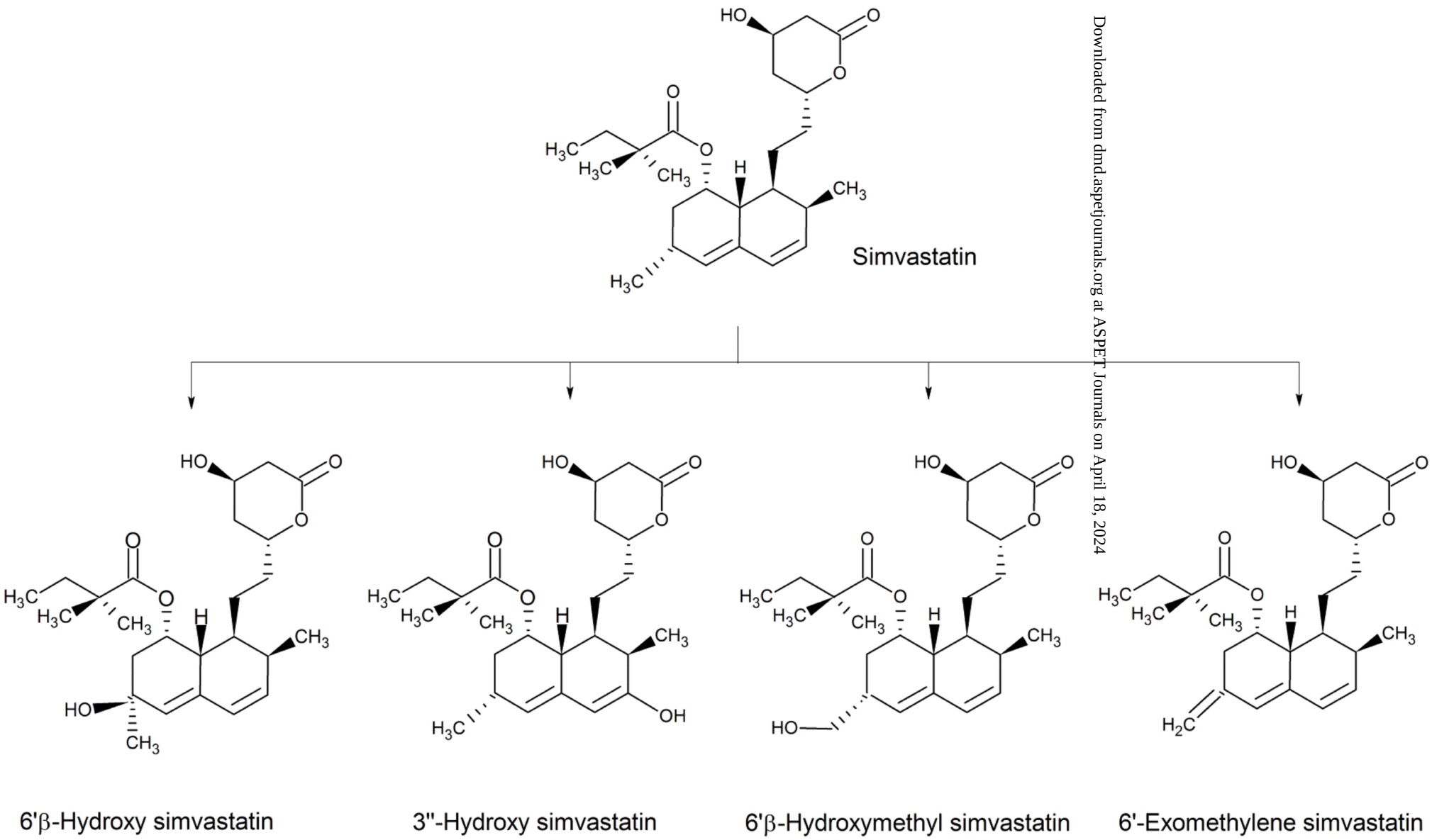

Figure 1

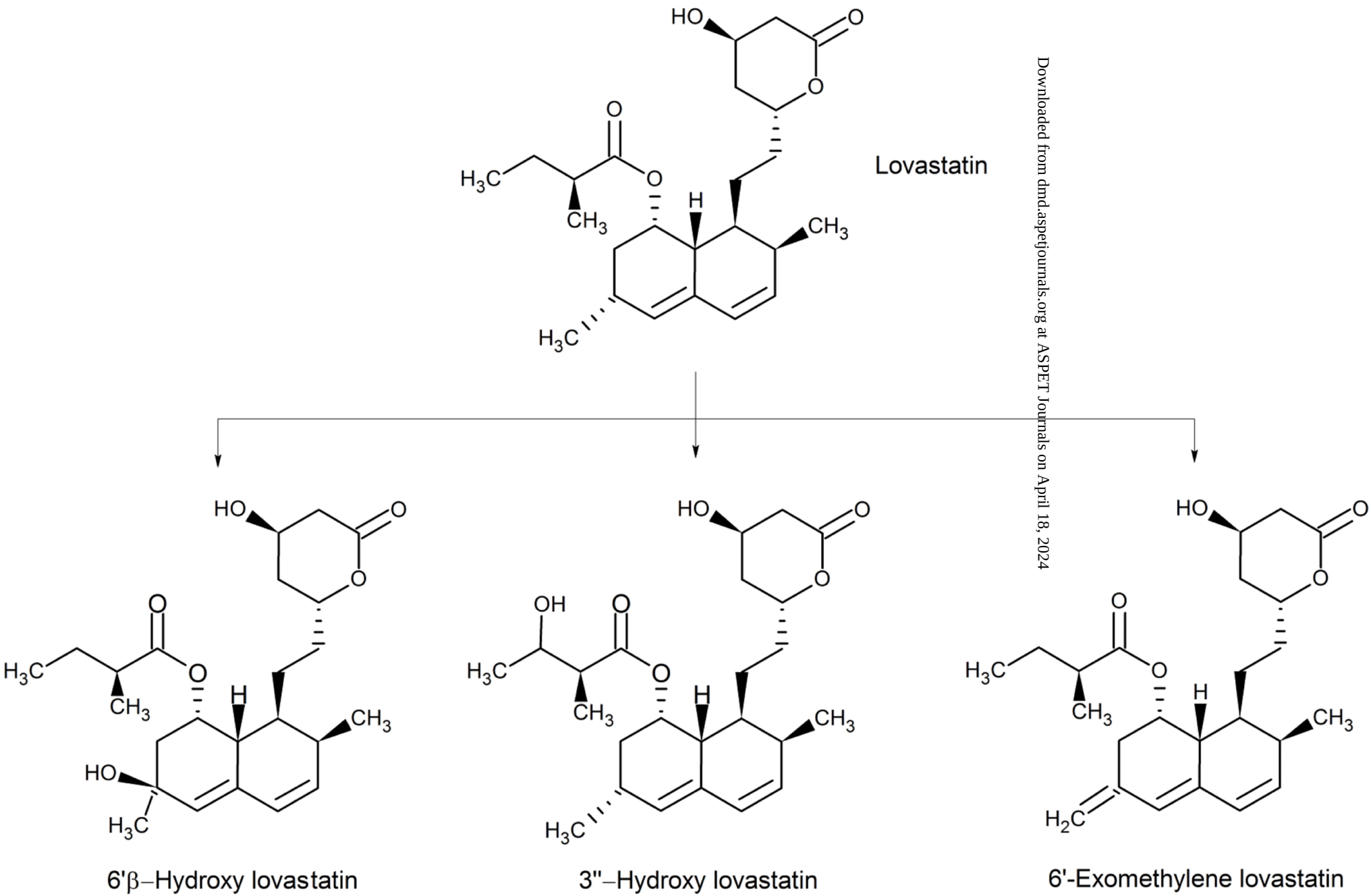

Figure 2

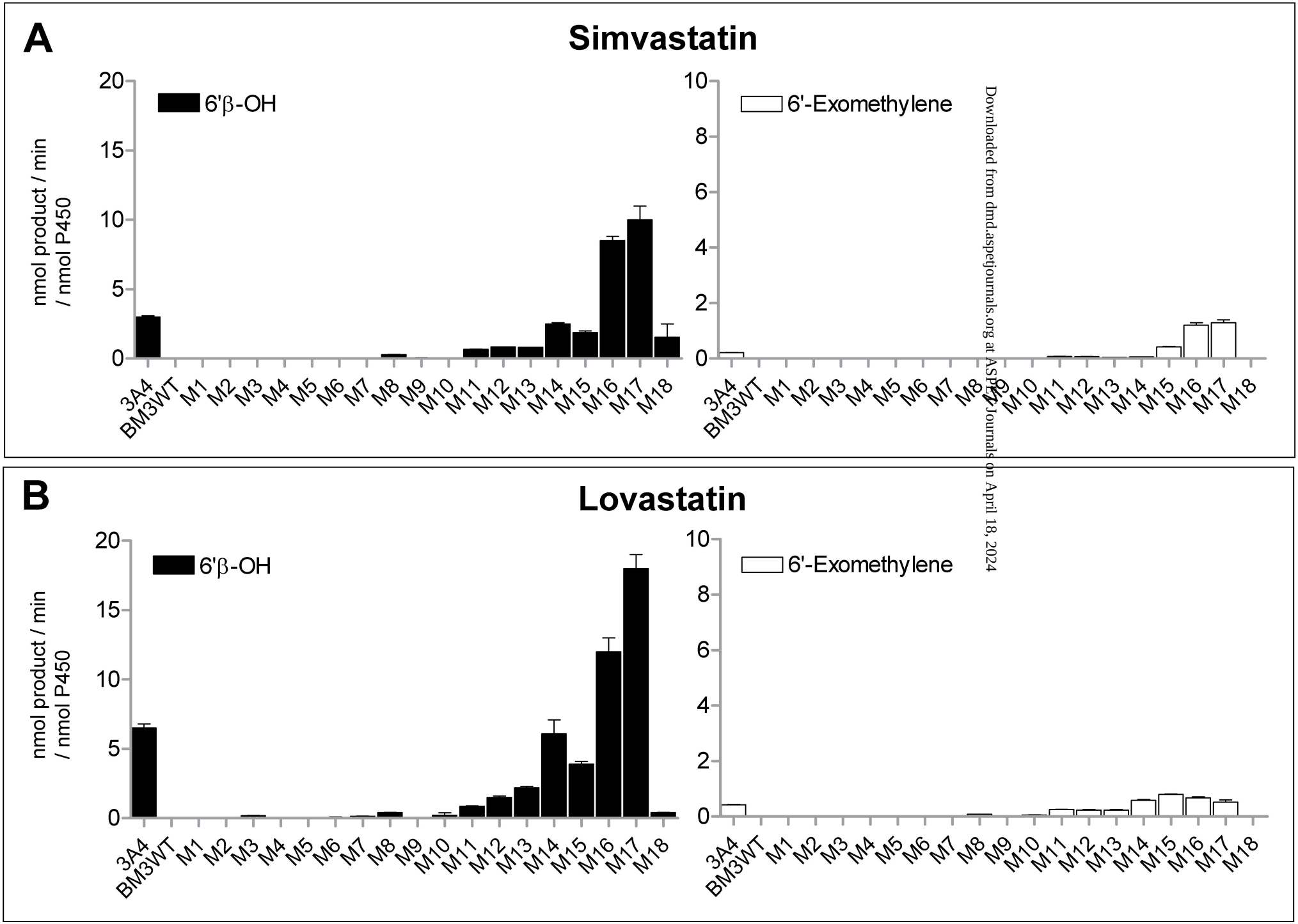

Figure 3

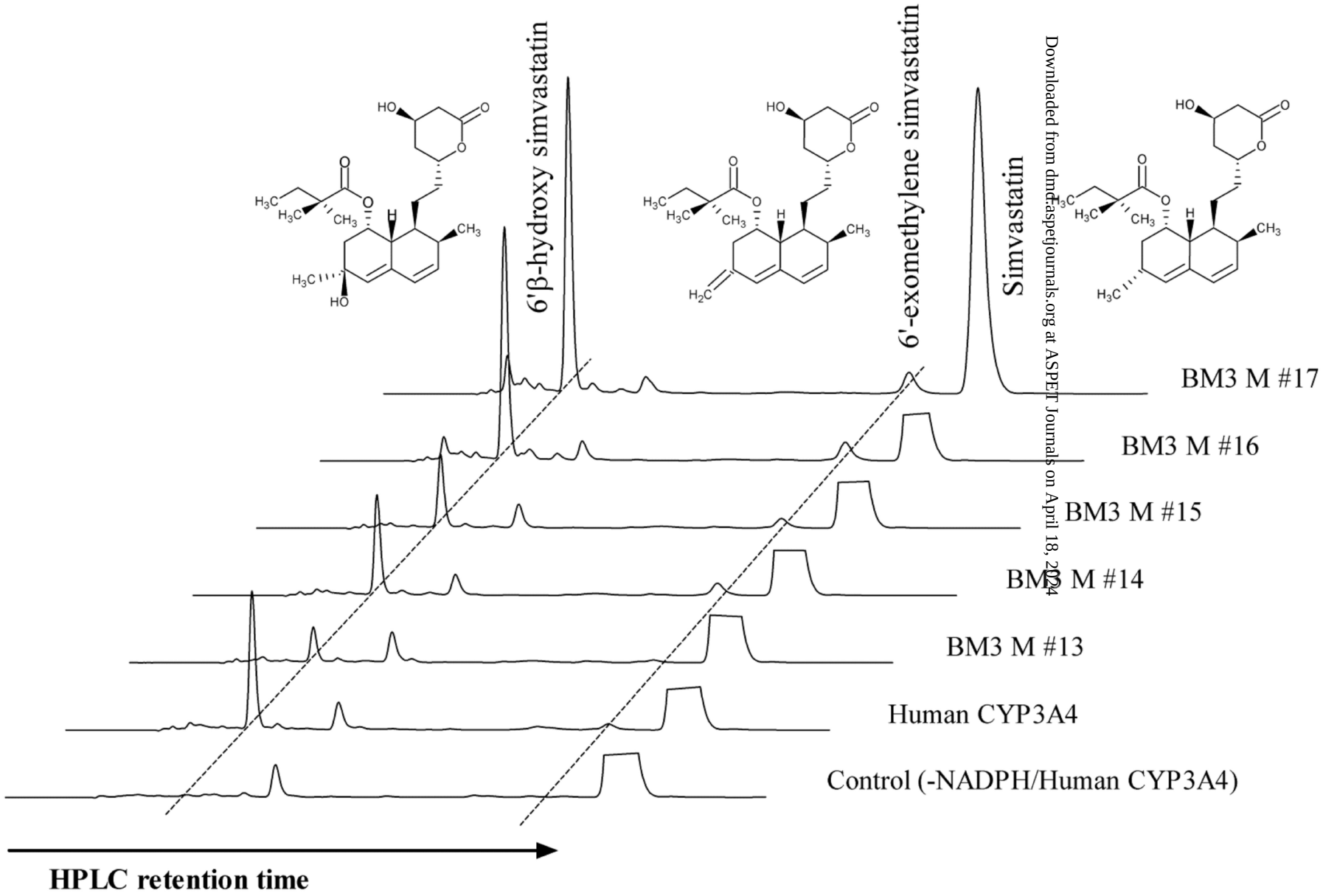

Figure 4

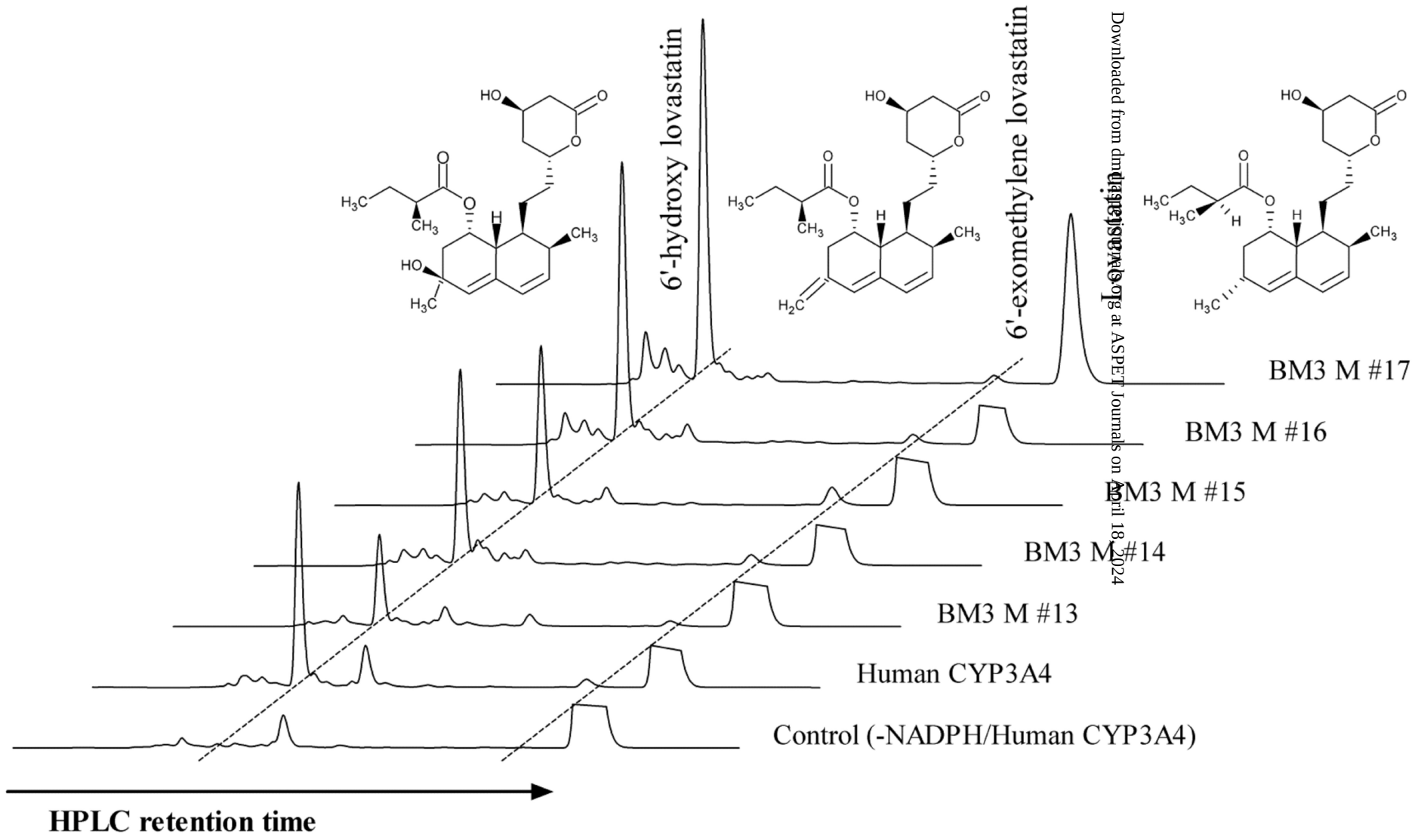

Figure 5

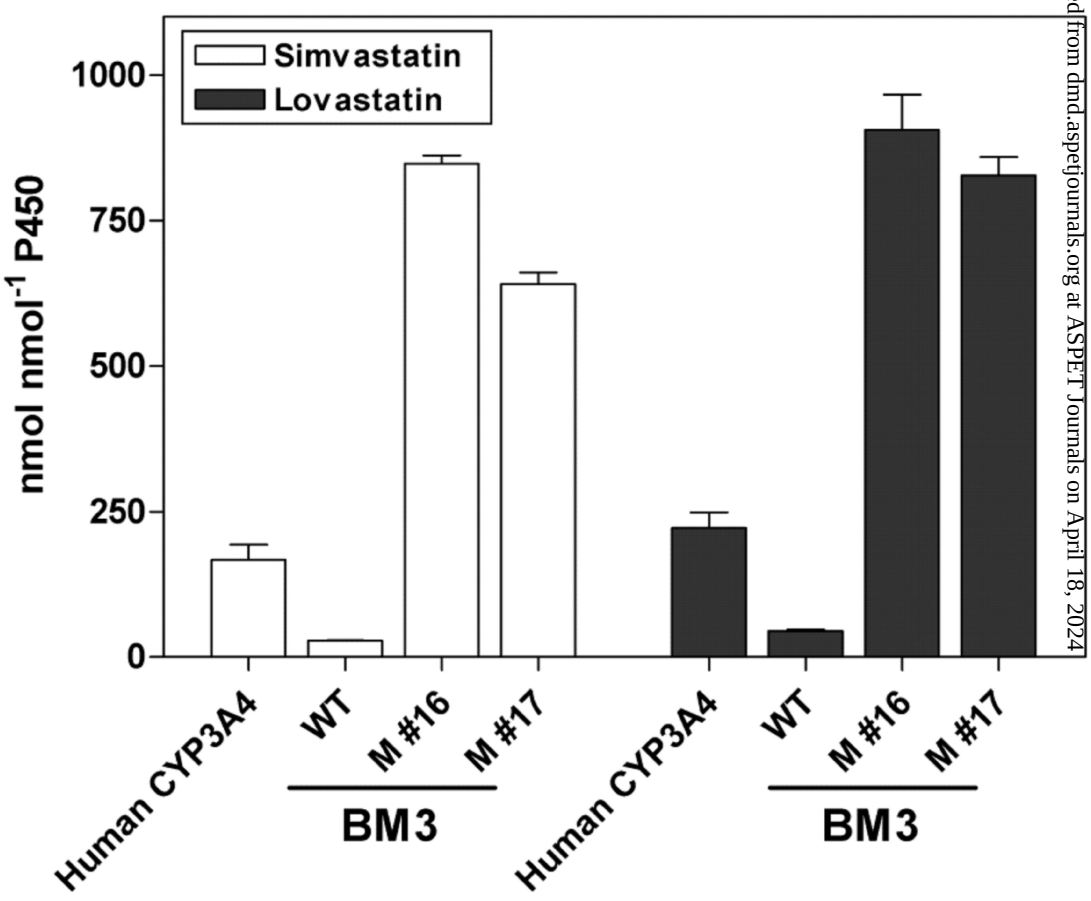

Figure 6

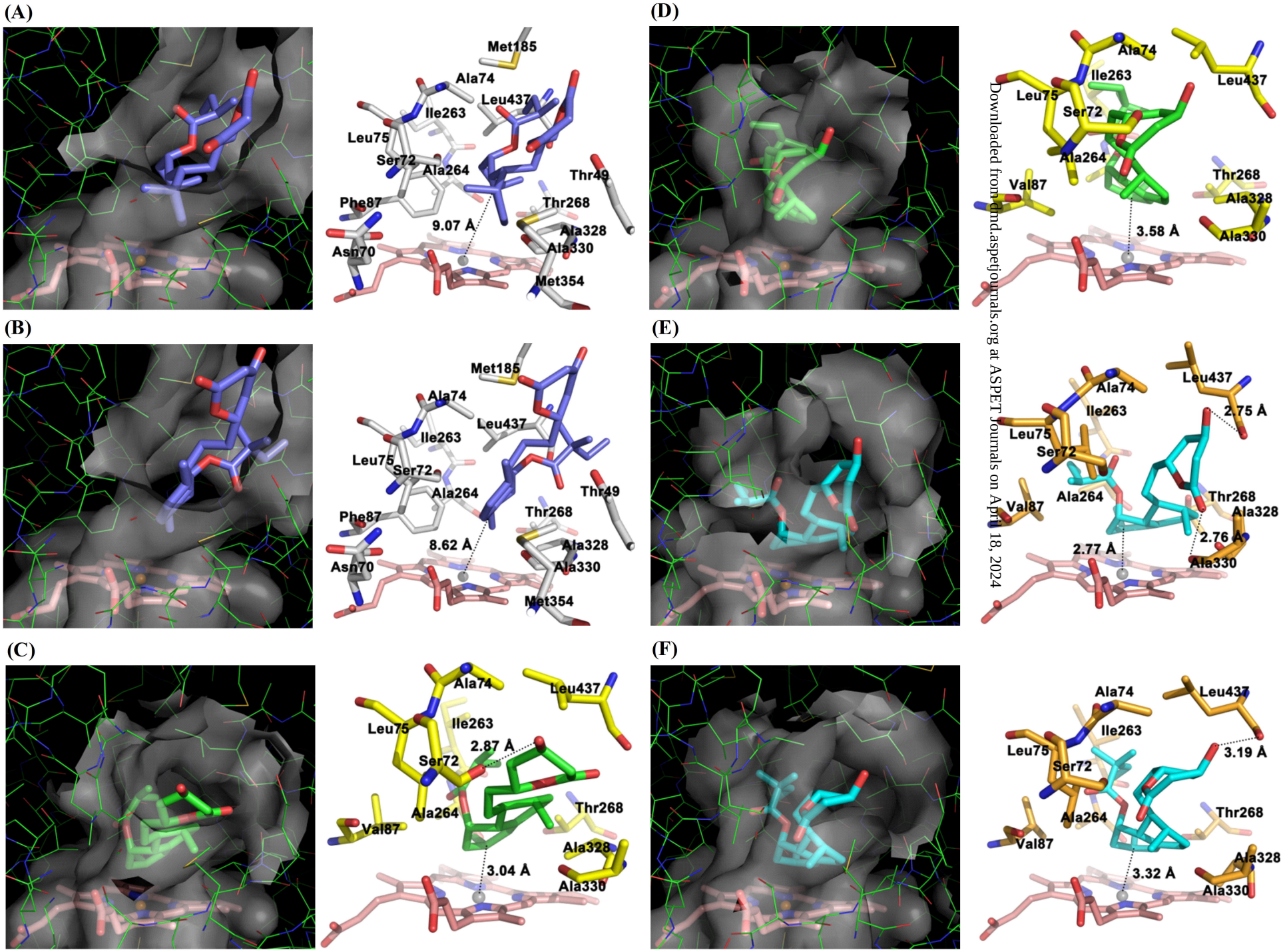

Figure 7

Supplemental Data to DMD MS #36392

Article title: Generation of Human CHIRAL Metabolites of Simvastatin and Lovastatin by bacterial CYP102A1 Mutants

Authors: Keon-Hee Kim, Ji-Yeon Kang, Dong-Hyun Kim, Sun-Ha Park, Seon Ha Park, Dooil Kim, Ki Deok Park, Young Ju Lee, Heung-Chae Jung, Jae-Gu Pan, Taeho Ahn, Chul-Ho Yun

Journal title: Drug Metabolism and Disposition

Supplemental Table S1. Mutated amino acid residues of CYP102A1 mutants used in this study

BM3 mutant	Mutated amino acid residues
#1	F87A
#2	A264G
#3	F87A/A264G
#4	R47L/Y51F
#5	R47L/Y51F/A264G
#6	R47L/Y51F/F87A
#7	R47L/Y51F/F87A/A264G
#8	A74G/F87V/L188Q
#9	R47L/L86I/L188Q
#10	R47L/F87V/L188Q
#11	R47L/F87V/L188Q/E267V
#12	R47L/L86I/L188Q/E267V
#13	R47L/L86I/F87V/L188Q
#14	R47L/F87V/E143G/L188Q/E267V
#15	R47L/E64G/F87V/E143G/L188Q/E267V
#16	R47L/F81I/F87V/E143G/L188Q/E267V
#17	R47L/E64G/F81I/F87V/E143G/L188Q/E267V
#18	F162I/K187E/M237I

Supplemental Table S2. Chemical shift of simvastatin

	Chemical shifts of simvastatin (ppm, $CDCl_3$)		
	13C	1H	HMBC (H->C)
1'-CH	36.59	1.68	C-8'a, C-2'
2'-CH	30.61	2.37	CH3-2'a, C-3', C-4', C-1', C-8'a
3'-CH	132.84	5.79	C-4a', C-1', C-2', CH3-2'a
4'-CH	128.37	5.99	C-5', C-8'a, C-2'
5'-CH	129.72	5.51	C-6', C-8'a, C-7',C-4'
6'-CH	27.25	2.44	
7'-CH2	32.86	2.44, 1.95	CH3-6'a, C-5'(weak), C-8', C-8a'
8'-CH	67.92	5.37	C-6', C-4'a
8'a-CH	37.49	2.26	C-2', C-1'(weak)
3-CH2	38.59	2.74,2.62	C-2, C-4
4-CH	62.75	4.38	
5-CH2	36.21	1.98, 1.69	C-6
6-CH	76.24	4.61	
7-CH2	32.94	1.89, 1.28	C-8, C-6, C-1'
8-CH2	24.29	1.49, 1.37	C-7, C-6, C-1', C-2'
3''-CH2	32.99	1.56	CH3-2'', C-1''(carbonyl), C-4'', C-2''(q)
4''-CH3	9.33	0.83	C-3'', C-2''(q)
2'a-CH3	13.87	0.89	C-2'
6'a-CH3	23.03	1.08	C-7',
2''-CH3	24.79, 24.75	1.27, 1.13	C-3'', C-1''(carbonyl), C-2''(q)
2''(quaternary)	42.99	X	
4'a(quaternary)	131.47	X	
2(carbonyl)	170.06	X	
1''(carbonyl)	177.80	X	

Supplemental Table S3. Chemical shift of 6'β-OH simvastatin.

	Chemical shifts of 6'β-OH simvastatin (ppm, $CDCl_3$)		
	13C	1H	HMBC (H->C)
1'-CH	36.32	1.67	
2'-CH	30.71	2.41	C-3', C-4', C-8'a, CH3-2'a
3'-CH	135.79	5.91	C-4'a, C-1', C-2'
4'-CH	127.68	5.99	C-4'a, C-5', C-8'a, C-2'
5'-CH	129.65	5.45	C-4', C-7', C-8'a
6'-CH	68.65	X	
7'-CH2	42.40	2.44(eq), 1.93(ax)	C-6', CH3-6'a
8'-CH	69.19	5.40	C-4'a
8'a-CH	37.62	2.34	
3-CH2	38.62	2.75, 2.63	C-2(carbonyl), C-4
4-CH	64.79	4.39	
5-CH2	36.20	1.96, 1.69	
6-CH	76.04	4.61	
7-CH2	32.76	1.88, 1.28	C-6, C-5
8-CH2	24.09	1.42	C-6, C-1', C-7
3"-CH2	33.03	1.56	C-1"(carbonyl), C-2", C-3", CH3-2", CH3-4"
4"-CH3	9.32	0.84	C-2"
2'a-CH3	13.57	0.89	C-3', C-1', C-2'
6'a-CH3	30.78	1.35	C-5', C-6', C-7'
2''-CH3	24.78, 24.76	1.14, 1.13	C-1"(carbonyl), C-2", C-3"
2"(quaternary)	43.07	X	
4'a(quaternary)	133.50	X	
2(carbonyl)	169.88	X	
1"(carbonyl)	177.50	X	

Supplemental Table S4. Chemical shift of lovastatin

	Chemical shifts of lovastatin (ppm, $CDCl_3$)		
	13C	1H	HMBC (H->C)
1'-CH	36.53	1.70	C-8'a, C-2', CH3-2'a
2'-CH	30.61	2.38	C-3', C-4', C-8'a, CH3-2'a
3'-CH	133.05	5.79	C-4'a, C-1', C-2', CH3-2'a
4'-CH	128.25	6.00	C-4'a, C-5', C-8'a, C-2', CH3-2'a
5'-CH	129.58	5.53	C-4', C-8'a, C-7', C-6'
6'-CH	27.39	2.45	C-8', CH3-6'a
7'-CH2	32.59	1.92	C-5', C-8'a, C-6', CH3-6'a, C-8'
8'-CH	67.85	5.39	C-4'a, C-6'
8'a-CH	37.20	2.27	C-4'a
3-CH2	38.52	2.73, 2.63	C-2(carbonyl), C-4, C-5
4-CH	62.52	4.37	
5-CH2	36.04	1.68, 1.97	C-6, C-4
6-CH	76.37	4.62	
7-CH2	32.88	1.87, 1.29	C-6, C-1', C-8, C-5
8-CH2	24.23	1.51, 1.39	C-6, C-1', C-7, C-2'
2"-CH	41.46	2.35	C-1", C-3",CH3-2", CH3-4"
3"-CH2	26.79	1.66, 1.44	C-1", C-2", CH3-2", CH3-4"
4"-CH3	11.71	0.88	C-2", C-3"
2'a-CH3	13.83	0.90	3', 1', 2'
6'a-CH3	22.79	1.08	5', 7', 6'
2''-CH3	16.22	1.11	C-1", C-2", C-3"
4'a(quaternary)	131.51	X	
2(carbonyl)	170.52	X	
1"(carbonyl)	176.92	X	

Supplemental Table S5. Chemical shift of 6'β-OH lovastatin.

	Chemical shifts of 6'β-OH lovastatin (ppm, $CDCl_3$)		
	13C	1H	HMBC (H->C)
1'-CH	36.19	1.69	CH3-2'a
2'-CH	30.57	2.40	C-3', C-4', C-1', CH3-2'a
3'-CH	135.90	5.92	C-4'a, C-1', C-2'(weak)
4'-CH	127.61	5.99	C-4'a, C-5', C-8'a
5'-CH	129.68	5.46	C-4', C-7', C-8'a
6'-CH	68.79	X	
7'-CH2	42.19	2.43(eq), 1.90(ax)	C'6, CH3-6'a
8'-CH	68.85	5.42	
8'a-CH	37.42	2.33	
3-CH2	38.61	2.74, 2.62	C-2(carbonyl)
4-CH	62.80	4.38	
5-CH2	36.27	1.94, 1.67	
6-CH	75.99	4.61	
7-CH2	32.74	1.87, 1.28	C-6
8-CH2	24.03	1.45	
2"-CH	41.40	2.37	C-1"(carbonyl),CH3-2", CH3-4"
3"-CH2	26.85	1.66, 1.46	C-1"(carbonyl), C-2", CH3-2", CH3-4"
4"-CH3	11.74	0.89	C-2", C-3"
2'a-CH3	13.59	0.90	C3', C-1', C-2'
6'a-CH3	30.74	1.34	C-5', C-7', C-2'
2''-CH3	16.29	1.12	C-1"(carbonyl), C-2", C-3"
4'a(quaternary)	133.50	X	
2(carbonyl)	169.99	X	
1"(carbonyl)	176.17	X	

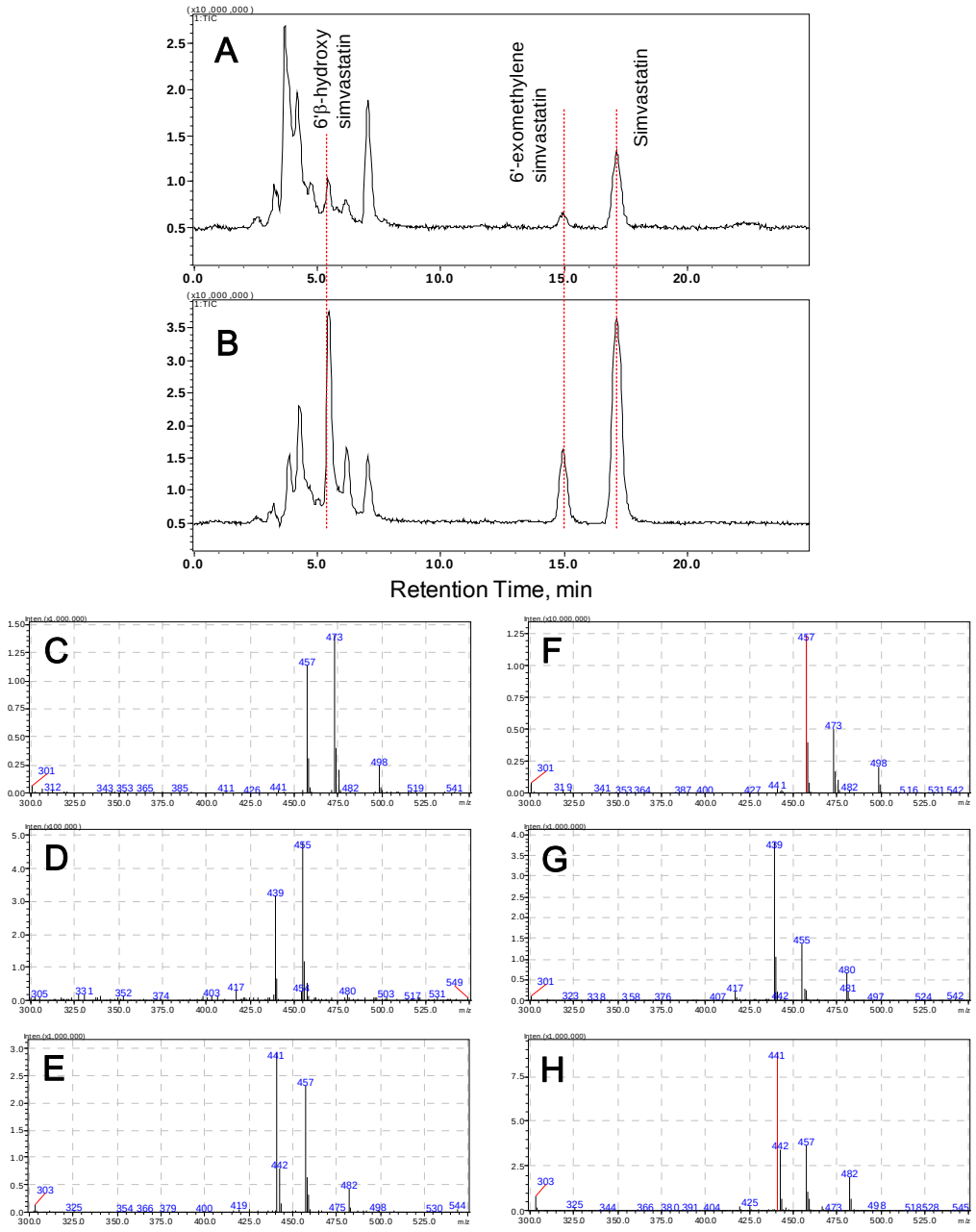

Supplemental Figure S1. LC-MS elution profile of simvastatin and its metabolites produced by CYP102A1 mutant #17 and human CYP3A4. TIC (total ion current) profiles of the metabolites generated by human CYP3A4 (A) and CYP102A1 mutant #17 (B) are shown. The mass spectra of the reaction samples showed peaks at 5.433 min (6'β-OH simvastatin), 14.933 min (6'-exomethylene simvastatin), and 17.100 min (simvastatin). Mass spectra of 6'β-OH simvastatin (C and F), 6'-exomethylene simvastatin (D and G), and simvastatin (E and H) produced by human CYP3A4 (C, D, and E) and CYP102A1 mutant #17 (F, G, and H) were shown. Calculated mass for $[M+Na]^+$, were 457, 439, and 441 for 6'β-OH simvastatin, 6'-exomethylene simvastatin, and simvastatin, respectively.

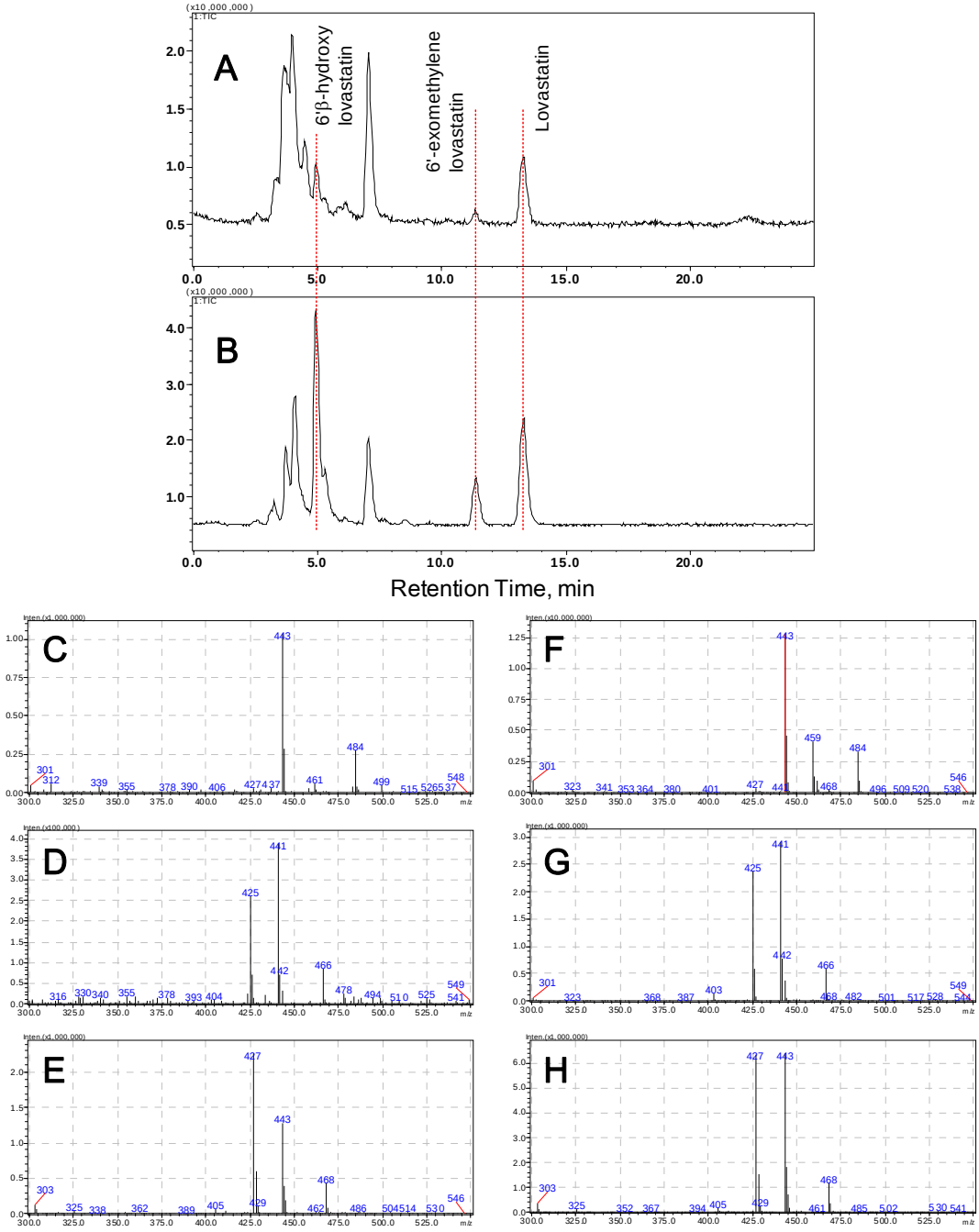

Supplemental Figure S2. LC-MS elution profile of lovastatin and its metabolites produced by CYP102A1 mutant #17 and human CYP3A4. TIC profiles of the metabolites generated by human CYP3A4 (A) and CYP102A1 mutant #17 (B) are shown. The mass spectra of the reaction samples showed peaks at 4.933 min (6'β-OH lovastatin), 11.367 min (6'-exomethylene lovastatin), and 13.267 min (lovastatin). Mass spectra of 6'β-OH lovastatin (C and F), 6'-exomethylene lovastatin (D and G), and lovastatin (E and H) produced by human CYP3A4 (C, D, and E) and CYP102A1 mutant #17 (F, G, and H) were shown. Calculated mass for $[M+Na]^+$, were 443, 425, and 427 for 6'β-OH lovastatin, 6'-exomethylene lovastatin, and lovastatin, respectively.

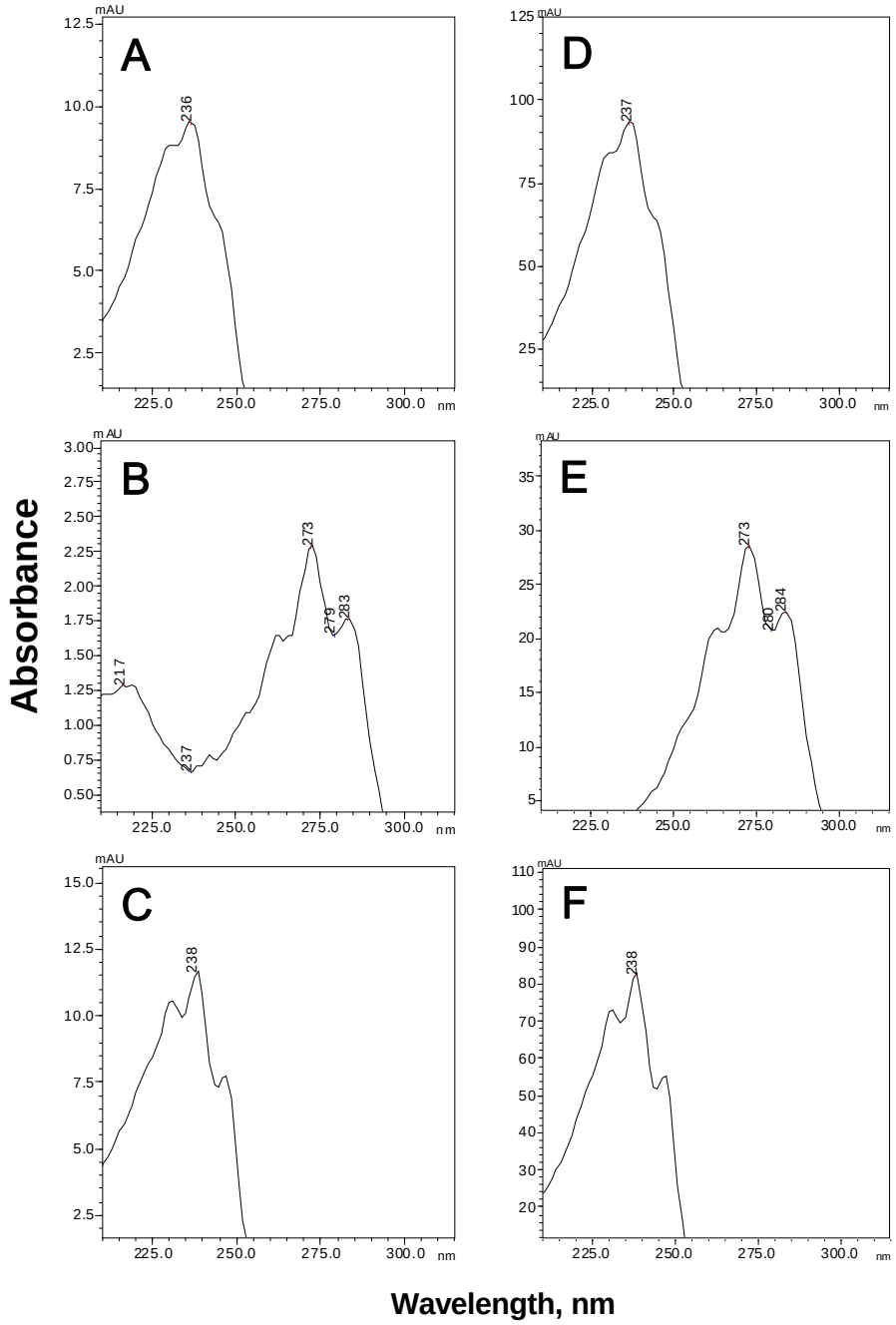

Supplemental Figure S3. Absorption spectra of simvastatin and its metabolites by human CYP3A4 (A, B, and C) and CYP102A1 mutant #17 (D, E, and F). The spectra were recorded in the mobile phase composition at which they were eluted from the column. A and D, 6'β-OH simvastatin; B and E, 6'-exomethylene simvastatin; C and F, simvastatin.

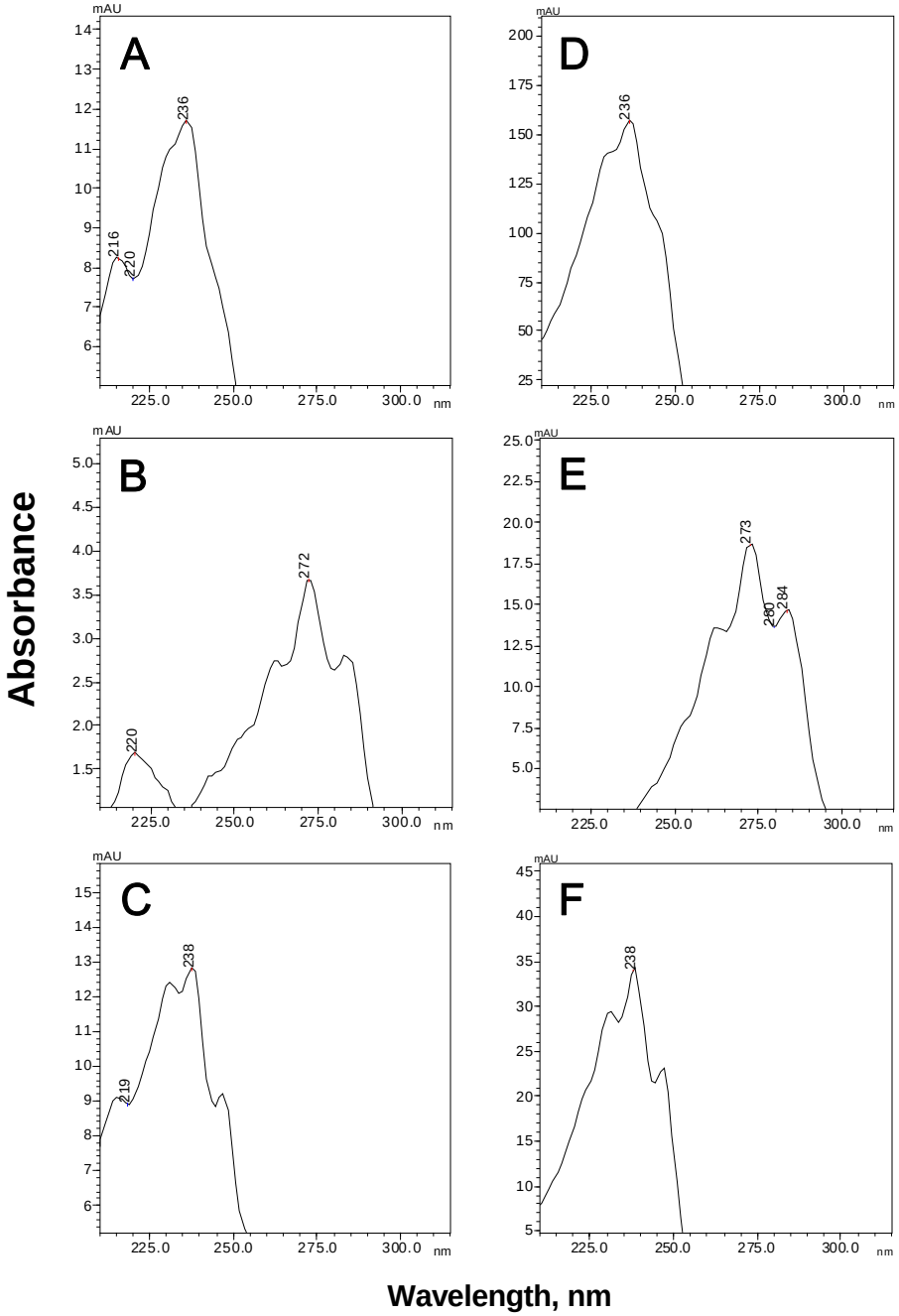

Supplemental Figure S4. Absorption spectra of lovastatin and its metabolites by human CYP3A4 (A, B, and C) and CYP102A1 mutant #17 (D, E, and F). The spectra were recorded in the mobile phase composition at which they were eluted from the column. A and D, 6'β-OH lovastatin; B and E, 6'-exomethylene lovastatin; C and F, lovastatin.

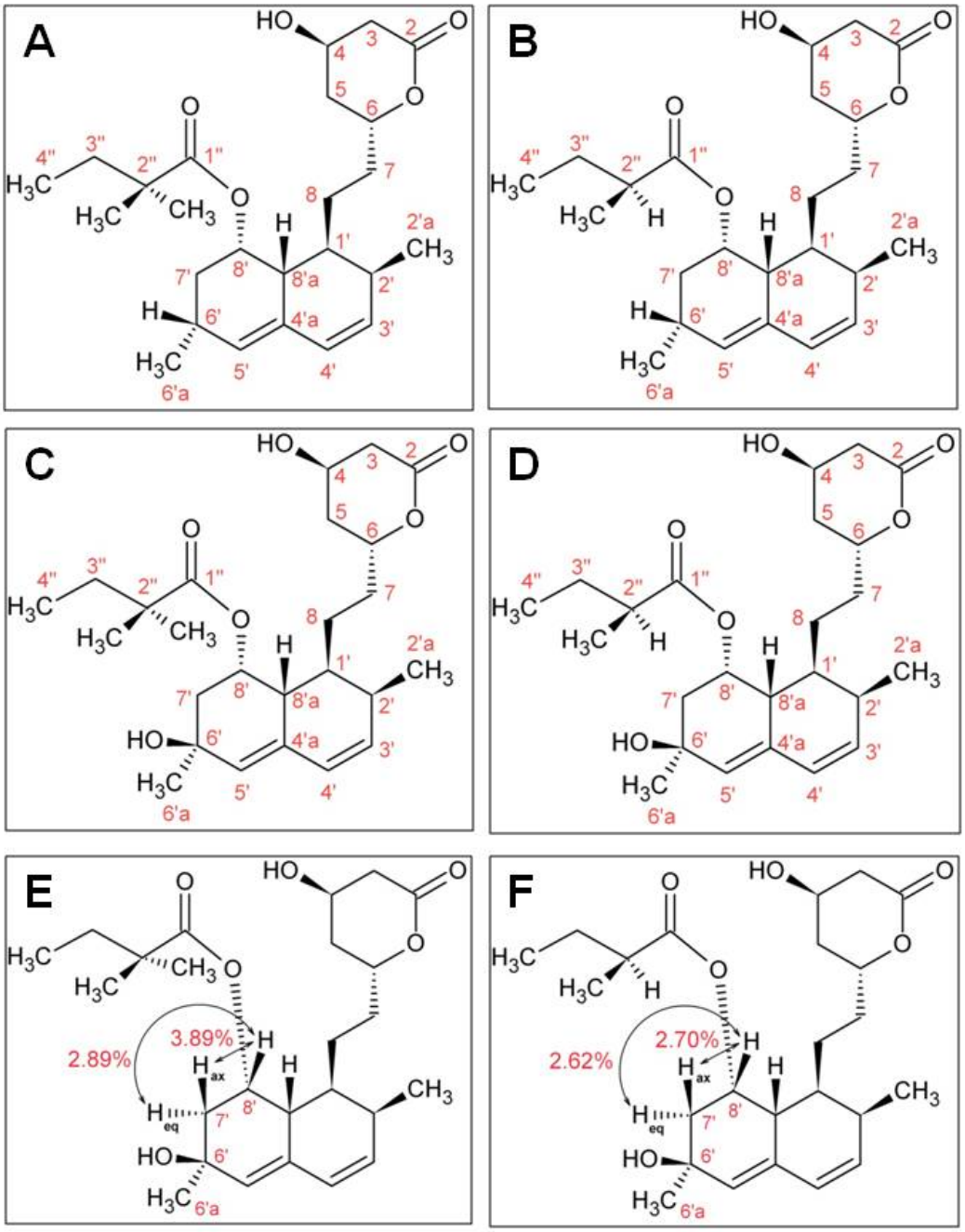

Supplemental Figure S5. Chemical structures of simvastatin (A), lovastatin (B), 6'β-OH simvastatin (C), and 6'β-OH lovastatin (D) for the NMR assignment. Key NOE results of 6'β-OH simvastatin (E) and 6'β-OH lovastatin (F) were shown respectively.

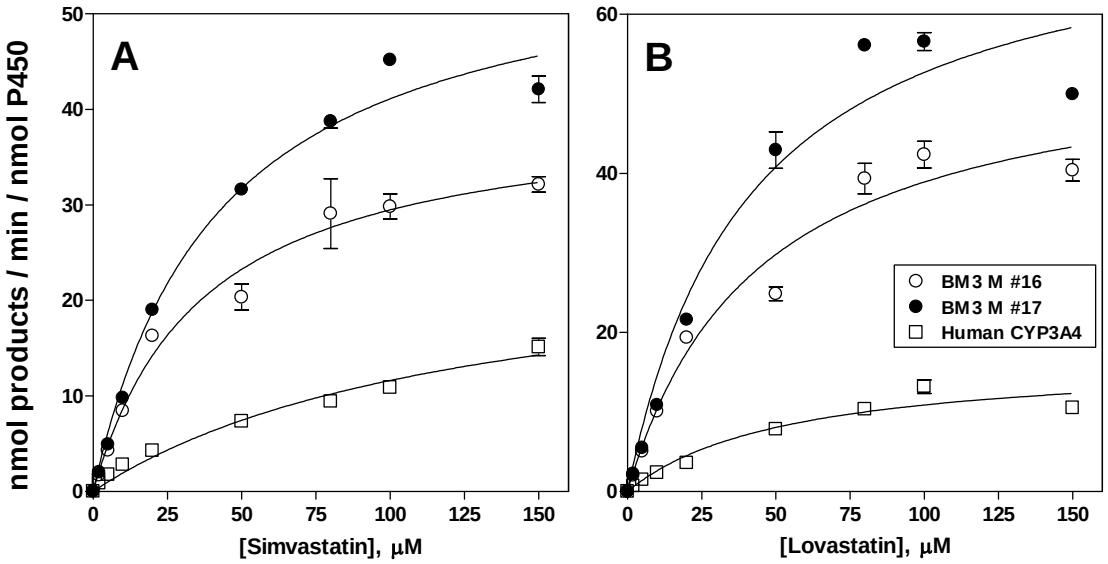

Supplementary Fig. S6. Kinetic parameters of 6'β-hydroxylation of simvastatin and lovastatin by CYP102A1 mutants and human CYP3A4. The 6'β-hydroxylation rates of simvastatin (A) and lovastatin (B) were measured in reaction mixtures consisting of 50 pmol CYP102A1 in 0.25 ml of 100 mM potassium phosphate buffer (pH 7.4) along with a specified amount of substrate (2 ~ 200 μM of statins).

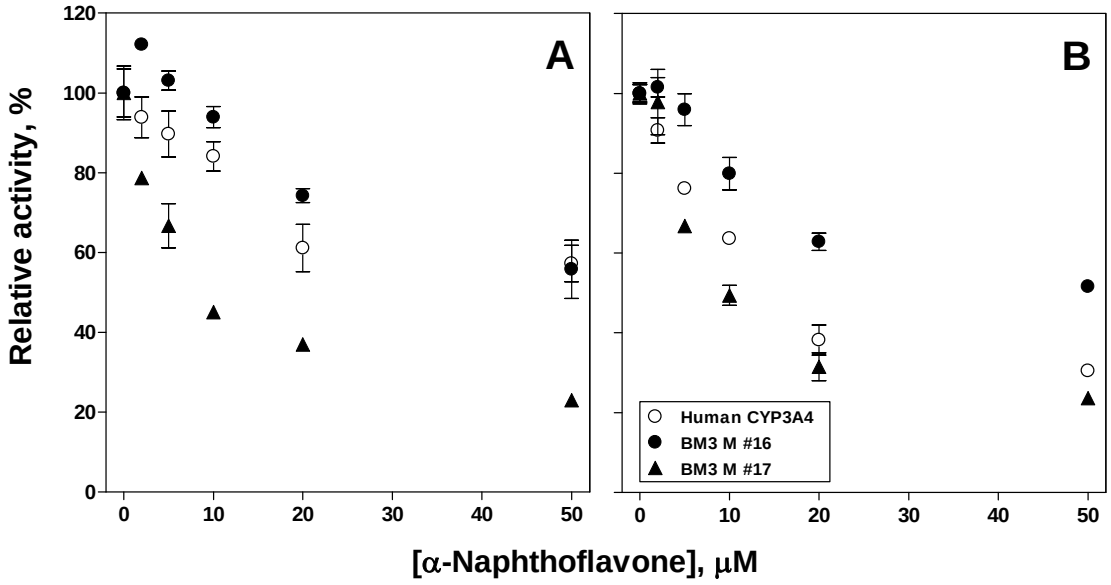

Supplemental Figure S7. Effect of αNF on 6'β-hydroxylation of simvastatin (A) and lovastatin (B), catalyzed by CYP102A1 mutants #16, #17, and human CYP3A4. Reaction mixtures consisted of 50 pmol P450, 100 mM potassium phosphate buffer (pH 7.4), a NADPH-generating system, and substrate (100 μM of simvastatin or lovastatin) in 0.25 ml of 100 mM potassium phosphate buffer (pH 7.4) in the presence of αNF (2 ~ 50 μM). Products were analyzed by HPLC, as described in Materials and Methods. In the case of human CYP3A4 activity assay, a control experiment of 50 pmol P450, 100 pmol NADPH-P450 reductase (CPR), 100 pmol cytochrome b_5, and 45 μM DLPC was used instead of 50 pmol CYP102A1.

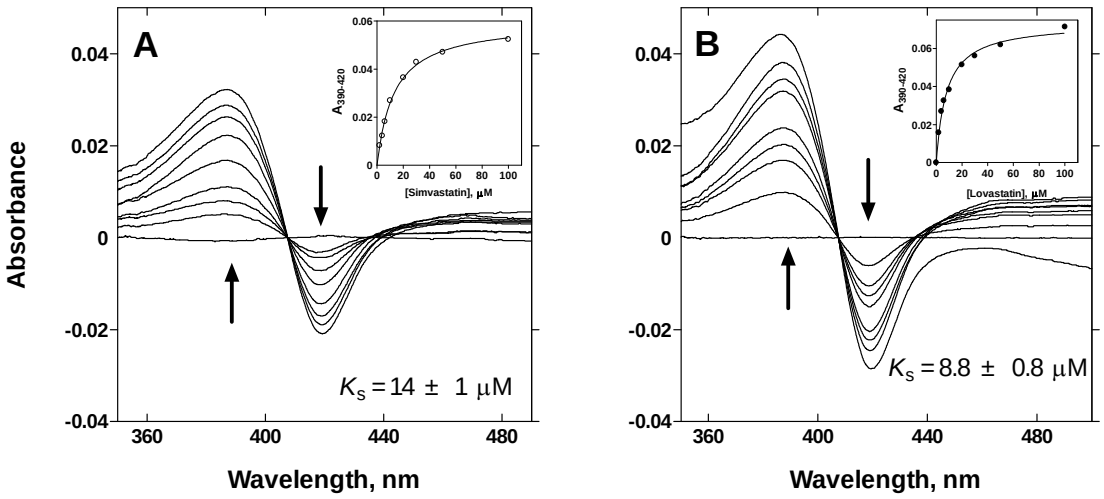

Supplemental Figure S8. Titration of ferric CYP3A4 with (A) simvastatin and (B) lovastatin. Human CYP3A4 (2 μM) was divided into each of two 1.0-ml glass cuvettes and baseline was set. Aliquots of substrates (simvastatin or lovastatin) in CH_3CN were added to the sample cuvette and equal volumes of CH_3CN were added to the reference cuvette. With increasing concentrations of chemicals, spectra were changed in the direction indicated by the arrows. The insets show the changes in absorbance, which were recorded using the dual wavelength mode, as a function of the indicated chemical concentration.

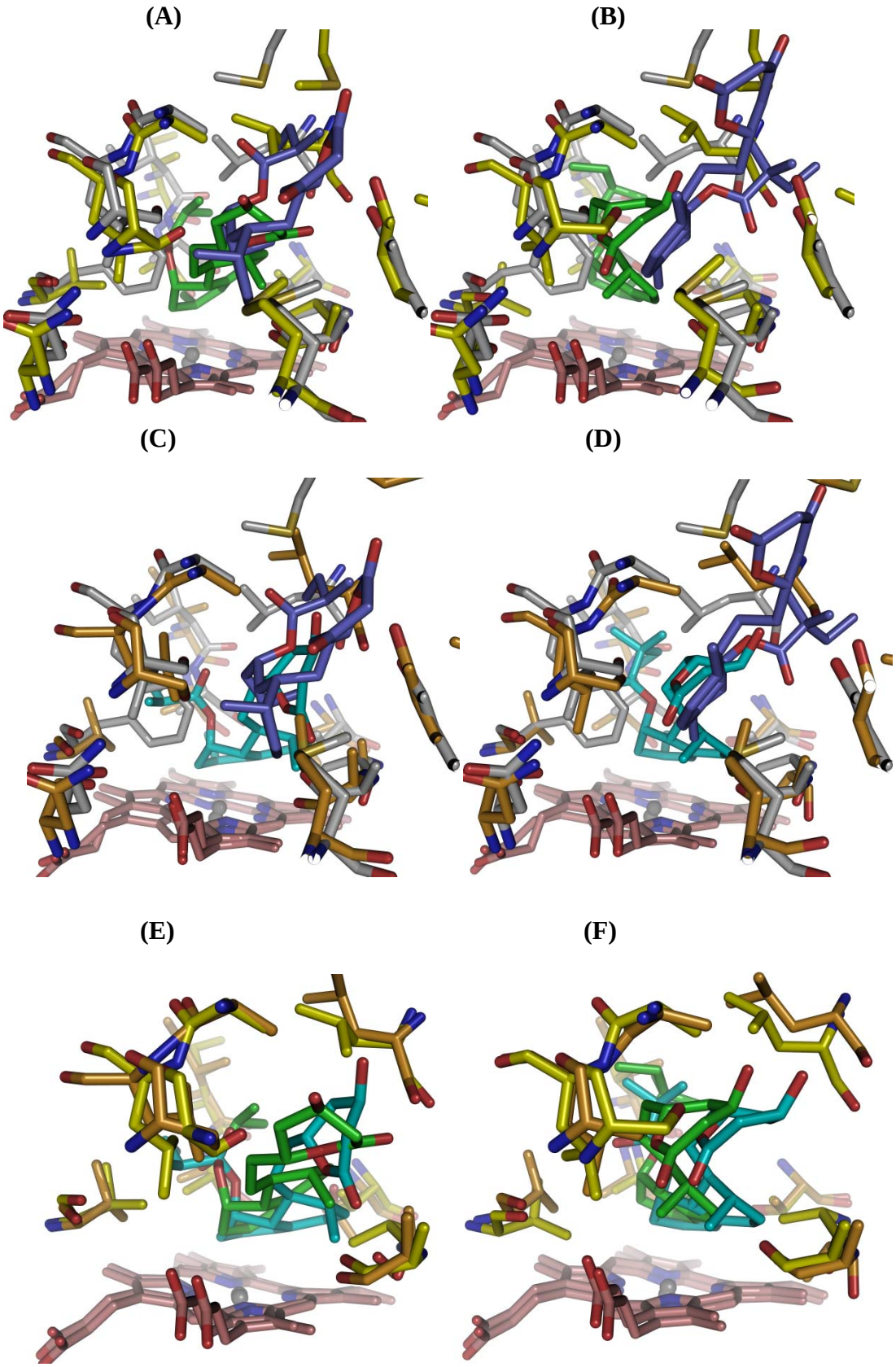
(A)
(B)
(C)
(D)
(E)
(F)

Supplementary Fig. S9. Superimposed averaged MD structure of CYP102A1 WT (grey)/LOV (cyan) and WT (grey)/SIM (cyan) complex with (A) mutant #16 (yellow)/LOV(green), (B) mutant #16 (yellow)/SIM(green), (C) mutant #17(orange)/LOV(cyan), and (D) mutant #17(orange)/SIM(cyan)complexes, respectively. Superimposed averaged MD structure of mutant #16 (yellow)/LOV(green) and mutant #16 (yellow)/SIM(green) complex with (E) mutant #17(orange)/LOV(cyan) and (F) mutant #17(orange)/SIM(cyan), respectively.